OPEN ACCESS

Journal of Engineering and Technology Research

July-December 2020
ISSN 2006-9790
DOI: 10.5897/JETR
www.academicjournals.org

ACADEMIC JOURNALS
expand your knowledge

About JETR

The Journal of Engineering and Technology Research (JETR) is a broad-based journal devoted to the advancement and dissemination of knowledge in all areas of engineering. The journal welcomes manuscripts in all areas of engineering such as electronics, artificial intelligence applications and innovations, information systems, kinetic processes in materials, strength of building materials among others.

JETR is a peer reviewed journal and publishes quarterly.

Indexing

The Journal of Engineering and Technology Research is indexed in Chemical Abstracts (CAS Source Index) and Dimensions Database

Open Access Policy

Open Access is a publication model that enables the dissemination of research articles to the global community without restriction through the internet. All articles published under open access can be accessed by anyone with internet connection.

The Journal of Engineering and Technology Research is an Open Access journal. Abstracts and full texts of all articles published in this journal are freely accessible to everyone immediately after publication without any form of restriction.

Article License

Memberships and Standards

Academic Journals strongly supports the Open Access initiative. Abstracts and full texts of all articles published by Academic Journals are freely accessible to everyone immediately after publication.

All articles published by Academic Journals are licensed under the Creative Commons Attribution 4.0 International License (CC BY 4.0). This permits anyone to copy, redistribute, remix, transmit and adapt the work provided the original work and source is appropriately cited.

Crossref is an association of scholarly publishers that developed Digital Object Identification (DOI) system for the unique identification published materials. Academic Journals is a member of Crossref and uses the DOI system. All articles published by Academic Journals are issued DOI.

Similarity Check powered by iThenticate is an initiative started by CrossRef to help its members actively engage in efforts to prevent scholarly and professional plagiarism. Academic Journals is a member of Similarity Check.

CrossRef Cited-by Linking (formerly Forward Linking) is a service that allows you to discover how your publications are being cited and to incorporate that information into your online publication platform. Academic Journals is a member of CrossRef Cited-by.

Academic Journals is a member of the International Digital Publishing Forum (IDPF). The IDPF is the global trade and standards organization dedicated to the development and promotion of electronic publishing and content consumption.

Contact

Editorial Office: jetr@academicjournals.org

Help Desk: helpdesk@academicjournals.org

Website: http://www.academicjournals.org/journal/JETR

Submit manuscript online http://ms.academicjournals.org

Academic Journals
73023 Victoria Island, Lagos, Nigeria
ICEA Building, 17th Floor,
Kenyatta Avenue, Nairobi, Kenya.

Table of Content

Vol. 12(1), pp. 1-11, July-December 2020
DOI: 10.5897/JETR2019.0676
Article Number: 10344E164317
ISSN: 2006-9790

http://www.academicjournals.org/JETR

ACADEMIC JOURNALS

Journal of Engineering and Technology Research

Full Length Research Paper

Prediction behavior of high frequency modulated by a 16 lengths Golay code undergoing honey attenuation

Vincent De Paul TEKOUA KOUEMENE* and Laurent BITJOKA

Laboratory of Energy, Signal, Imaging and Automation (LESIA), National School of Agro-industrial Sciences, The University of Ngaoundere, P. O. Box 455, Ngaoundere, Cameroon.

Received 25 September, 2019; Accepted 23 April, 2020

Optical microscopic analysis of honey is time consuming due to the period needed to prepare samples. Time reduction could be achieved with ultrasound microscopy. This paper investigates the behavior of 125 MHz signal modulated by 16-bits Golay code spread out through a honey sample containing pollen. A bipolar phase shift keying (BPSK) modulation of 125 MHz frequency by 16-bits Golay code was implemented in Simulink/Matlab environment. The frequency implemented was set up considering the acoustic properties of honey containing pollen, the thickness of the sample and the size of pollen. At this frequency, the evaluated attenuation coefficient of honey containing pollen was 0.135 dB/µm/MHZ$^{(\gamma=1)}$; it depends on the power factor γ related to the scattering medium, and the delay induces by the size of pollen. The impact of these parameters, added to 5dB White Gaussian Noise on 200 V magnitudes BPSK Golay sequences, decreased the autocorrelation function magnitude from 8×10^4 V to 1.5×10^4 V. The width (Wd) decreases from 4 ns at 0.135 dB/µm/MHz$^{(\gamma=1)}$ to 3.5 ns at 16.875 dB/µm/MHz$^{(\gamma=2)}$, when the Pulse Side lobe Level (PSL) increases from -22.79 dB at 1.509 dB/µm/MHz$^{(\gamma=1)}$ to -9.54 dB at 16.875 dB/µm/MHz$^{(\gamma=2)}$.

Key words: Ultrasound, honey, attenuation coefficient, Golay code, BPSK modulation, autocorrelation function.

INTRODUCTION

Rheological analysis of honey is often realized using ultrasound at low frequency. It focuses on the determination of the speed of ultrasound, the viscoelastic moduli and contributes to the control quality of the given sample (Awad et al., 2012; Mehryar et al., 2013; Chandrapala, 2015). During their propagation in a medium, the ultrasound undergoes phenomena such as absorption, diffusion and dispersion. These phenomena are amplified with the increase of the frequency and the nature of the medium. Studies have shown that to size up the operational ultrasound frequency, a compromise must be made between resolution and penetration, which are two important parameters to be considered to ensure the quality of the characterization. Indeed, the resolution increases as the frequency goes up high; in the same time, the penetration decreases as the frequency increases (Berson et al., 1994; Clair et al., 2000). Characterization of an environment or a structure can be

*Corresponding author. E-mail: vintekoueme@gmail.com. Tel: 00 (237) 699 796 831.

qualitative (imaging of the structure) or quantitative (evaluation of the speed of ultrasound in the milieu, also the evaluation of the attenuation coefficient, and the evaluation of the thickness of the considered structure). The Quantitative analysis can be performed without introducing any chemical or biological damage in the sample and can give the way to appreciate the interfaces in the structure under analysis (Berger and Laugier, 1992; Chandrapala, 2015).

One of the acoustic parameter that is not well-known, but is considered important when carrying quantitative characterization of honey is the attenuation coefficient. Indeed, Laux et al. (2011) measured the amplitude of the first echo in chestnut honey at 15.7% of moisture using 200 V magnitude ultrasonic signal at 13.5 MHz but they could not be able to measure the amplitude of the second echo in the same sample. The absorption loss coefficient, which is nothing other than the attenuation coefficient was not determined (Laux et al., 2011). By developing a non-destructive and non-invasive method, using ultrasonic spectrometry, Kulmyrzaev and McClements (2000) measured the phase and amplitude of the reflected signal at the honey surface at various concentrations, as well as the viscous dynamic and the Elastic dynamic moduli. The operational frequency varied between 5 MHz and 10 MHz. Results on rheological analysis of honey were produced but did not come to the determination of the attenuation coefficient (Kulmyrzaev and McClements, 2000). Cereser and Laux (2010a) has developed a method based on the measurement of the complex reflection coefficient at the interface between an elastic material and a viscoelastic material. This method has allowed the determination at 10 MHz of the elastic dynamic modulus and the viscous dynamic modulus of honey, without a determination of the attenuation coefficient of that honey (Cereser and Laux, 2010a). Nevertheless, the mathematical expression of these two module allows the expression of this attenuation, which is known to be proportional to the reverse of the deep penetration of the ultrasound in the medium as indicated in literature (Cereser and Laux, 2010b). The measurement of the loss absorption coefficient requires the identification of at least two interfaces in a given sample and their acoustic parameters known (McClements and Fairley, 1992). If honey is considered as a medium with more than one interface, it is possible to model the amplitude of the signal crossing the identified interfaces, and to calculate the attenuation coefficient of each of them. This method was implemented by McClements and Fairley (1991); McClements and Sundaram (1997) with an ultrasonic reflectometer to determine the viscosity, the attenuation coefficient as well, as the acoustic impedance of some food and liquids at the frequency of 2.1 MHz but did not carry out the study on honey (McClements and Fairley, 1991; McClements and Sundaram, 1997). To mark this lack of information on the value of the attenuation coefficient of honey, Szabo (2014) has presented a table of the acoustic parameters of parts of the human body and some liquids including honey without indicating the value of its attenuation coefficient (Szabo, 2014). This work considers a sample of honey containing pollen and evaluates the acoustics parameters of honey and pollen. Those parameters lead to the dimension of 350 MHz frequency for the qualitative characterization of honey. One problem faced was the transmission of this frequency considering the power law of the attenuation. Indeed, high frequency induced better resolution of the imaging, but at the same time, attenuation increases and the penetration of the characteristic signal in the sample is poor. To overcome this difficulty, the frequency was reduced to 125 MHz and has considered the coded signal for the quantitative characterization of honey containing pollen. In literature, Golay code presents good characteristics in the transmission of signal, such as the improvement of signal-to-noise ratio, the reduction of side lobes in the autocorrelation function and also the elongation of Golay code can improved the penetration of encoded signal in the sample (Nowicki et al., 2007; Alvaro et al., 2007; Trots et al., 2008). The encoded signals using complementary Golay code are more developed for RADAR and biomedical imaging process (Nowicki et al., 2003; Vijay, 2011). In those files, the transmission of encoded signal is usually made simultaneously in the medium for it characterization using a transducer having more than one piezoelectric element. In this case, any sequence of encoded signal will arrive at the same time on the medium (Shin et al., 2008). For this study the transducer has one piezoelectric element and the expectation is to obtain comparative results.

MATERIALS AND METHODS

This study is based on honey containing pollen since the natural presence of pollen in honey can give information on its geographical origins. Also, the dimension of the pollen cannot be negligible if the thickness of the sample to be analyzed is considered. So, modeling the attenuation coefficient of honey containing the pollen is the first stage to be carried out. After this, the algorithm of Golay code just as evaluation parameters will be presented, and the mathematical equations of BPSK modulation of a high frequency by the 16 bits Golay code and its propagation in an impulse response medium, will be established. These equations will be implemented in the Simulink/matlab environment and the results of the simulations of the disturbances of the attenuation coefficient of honey containing pollen that were found on the propagation of Golay code sequences, will be analyzed.

Modeling of the attenuation coefficient of honey containing pollen

Considering D(µm) as the thickness of honey sample containing pollen and knowing that the largest pollen size has a diameter of 250 µm (Dahdouh, 2011; Ferrus, 2012), it is agreed that the honey/pollen interface has a minimum thickness of (D-250) µm, if pollen is found at the bottom of the container. Assuming that there

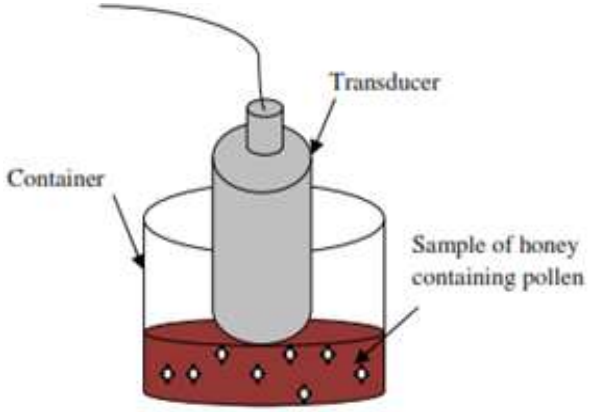

Figure 1. Illustration of principle for the evaluation of attention coefficient of honey containing pollen.

is one pollen in the ultrasonic propagation field, in the focal area of the transducer, the magnitudes would be modeled across these different interfaces during the propagation of emitted signal. The principle is depicted in Figure 1. From this illustration one can identify the following interfaces:

(i) The honey/pollen (upper side) interface, designated by MP_s;
(ii) The pollen (lower side)/honey interface, designated by P_iM;
(iii) The honey/container interface, designated by MB.

These three interfaces allow the writing of the ultrasound attenuation relationships in the medium as follows:

$$A_{MP_s} = A_i R_{MP_s} e^{-2\alpha_m d} \quad (1)$$

$$A_{P_iM} = e^{-2\alpha_m d}\left(1-R_{MP_s}\right)^2 R_{P_iM} A_i e^{-2\alpha_p D} \quad (2)$$

$$A_{MB} = e^{-2\alpha_m d} e^{-2\alpha_p D}\left(1-R_{MP_s}\right)^2 \times \left(1-R_{p_iM}\right)^2 R_{MB} A_i e^{-2\alpha_m d} \quad (3)$$

Where A_i is the initial amplitude emitted by the transducer, A_{MPs} is the amplitude at honey/pollen (upper side) interface, A_{PiM} is the amplitude at the pollen (lower side)/honey interface, R_{MPs} is the reflection coefficient at the honey/pollen (upper side) interface; R_{PiM} is the reflection coefficient at the pollen (lower side)/honey interface; α_m is the attenuation coefficient of honey; α_p is the attenuation coefficient of pollen; d (D-250) µm is the thickness of honey interface; D is the thickness of the honey sample containing pollen. The attenuation coefficient of honey α_m is obtained from Equations 1 and 2:

$$\alpha_m = \frac{1}{2d}\ln\frac{A_i}{A_{MP_s}} R_{MP_s} \quad (4)$$

If

$$R_{MP_s} = R_{P_iM} = \left(\frac{\rho_1 c_1 - \rho_2 c_2}{\rho_1 c_1 + \rho_2 c_2}\right)^2 \quad (5)$$

Where, C_1, ρ_1 and C_2, ρ_2 are respectively the speed of ultrasound and density for honey and pollen. For honey, C_1 equals to 2030 m/s and, ρ_1 equals to 1420 kg/m^3 (Szabo, 2014). The density ρ_2 of the pollen of "Amaranthus Palmeri" is equal to1218 kg/m^3 (Sosnoskie et al., 2009) and the evaluated velocity C_2 of ultrasound in the pollen is equal to 1570 m/s (Aouzale et al., 2010; Duclos et al., 2009; Duclos et al., 2010). The attenuation coefficient of pollen is obtained from equations 2 and 3, and leads to the following relation:

$$\alpha_p = \frac{1}{2D}\ln\left[\frac{\left(1-R_{MP_s}\right)^2 * A_{MP_s}}{A_{P_iM}}\right] \quad (6)$$

Considering that the density of pollen is identical for all the pollen sizes, the reflection coefficient will be determined and will proceed to the determination of the attenuation coefficient of the honey and the pollen. This hypothesis is justified if there is only one type of pollen in the considering sample of honey. Laux et al. (2011) has realized an experiment that permitted to measure the amplitude of the first echo in a given sample of monofloral chestnut honey, (Laux et al., 2011). They emitted an ultrasound of 13.5 MHz with 200 V Amplitude in the sample haven 400 µm thickness, at different temperatures and they measured the amplitude of echo. The value of 150 mV was measured at 23.5°C (Laux et al., 2011). Attenuation coefficient is given in Np/µm and Knowing that α(dB)=8,6886α(Np), at the operational frequency, the result is in dB/µm/MHZ$^\gamma$ (Szabo, 2014). The relationship between attenuation coefficient and frequency is given by the following equation:

$$\alpha_{mp} = \alpha_1 * (f)^{\gamma} \quad (7)$$

Algorithm of generating Golay code

Golay code is a pair of binary code, belonging to the large family of complementary codes. It consists of two sequences with the same length L, whose autocorrelations have identical side lobes in absolute value but opposite signs. The autocorrelation function obtained by summing up the two previous sequences has a main lobe with amplitude equal to 2L, and the secondary lobes with amplitude equal to zero (Edgar et al., 2008). Sequences a(n) and b(n) are Golay codes of length L if and only if the following autocorrelation function is checked (Shin et al., 2008; Edgar et al., 2008).

$$a(n) * a(-n) + b(n) * b(-n) = 2L\delta(n) \quad (8)$$

(∗) is the convolution operator and δ (n) is the Kroneker of the Delta function.
If $a_L(n)$ and $b_L(n)$ are Golay codes, $a_{2L}(n)$ and $b_{2L}(n)$ are also Golay codes obtained by concatenation.

$$\begin{cases} a_{2L}(n) = [a_L(n)\ \ b_L(n)] \\ b_{2L}(n) = [a_L(n)\ \ -b_L(n)] \end{cases} \quad (9)$$

Therefore, sequences of Golay codes can be built recursively knowing the initial values. For example $a_2(n) = [1\ 1]$ and $b_2(n) = [1\ -1]$. For a length $L = 16 = 2^4$ these sets are as follow (Nowicki et al., 2007).

$$\begin{cases} a_2(4) = [1\ 1\ 1\ -1\ 1\ 1\ -1\ 1\ 1\ 1\ 1\ -1\ -1\ -1\ 1\ -1] \\ b_2(4) = [1\ 1\ 1\ -1\ 1\ 1\ -1\ 1\ -1\ -1\ -1\ 1\ 1\ 1\ -1\ 1] \end{cases} \quad (10)$$

According to Trots et al. (2008), the comparison of results obtained for different lengths of Golay coded (8 bits; 16 bits; 32 bits and 64 bits), 16 bits Golay codes seems to be a good compromise because using longer coded sequences leads to increase the blain area in front of the transducer and consequently, the dead zone in the final signal. In the other hand, a short sequence does not assure sufficient Signal to noise ratio (SNR) (Trots et al., 2008). In RADAR and clinical applications, the general definitions of the following quality factors are used to evaluate Golay code application: Peak Side lobe Level (PSL), Integrated Side lobe Level (ISL) and the pulse width (Wd) of the autocorrelation function. These quality factors are often used in order to analyze the volume of the signal side lobes at the filter output (Misaridis et al., 2000; Vijay, 2011; Alejos et al., 2008). The PSL and the Wd parameters only will be evaluated in this work.

(i) Peak Side lobe Level (PSL) is the ratio of the maximum of the side lobe amplitude to main lobe amplitude;

$$PSL = 20\log_{10}\left[Max\left(\frac{r(i)}{r(0)}\right)\right], i \neq 0 \quad (11)$$

(ii) The width of the autocorrelation function (Wd) is the band pass of the main lobe.

Mathematical expression of the characterization of a medium using Golay encoded signal and the application of an adapted filter

G_1 ($g_1(n)$, n = 1,2, ..., N)) and G_2 ($g_2(n)$, n = 1,2, ..., N)) being complementary sequences of Golay, G'_1 ($g_1(-n)$, n = 1,2, ..., N)) and G'_2 ($g_2(-n)$, n = 1,2, ..., N)) are the corresponding replicas, and they all represented the temporal expressions of Golay code. The modulations of these sequences with a high frequency are given as follows:

$$T_1(t) = G_1(t)e^{j2\pi f_0 t} \quad \text{(a)}$$

$$T_2(t) = G_2(t)e^{j2\pi f_0 t} \quad \text{(b)}$$

$$T'_1(t) = G'_1(t)e^{-j2\pi f_0 t} \quad \text{(c)}$$

$$T'_2(t) = G'_2(t)e^{-j2\pi f_0 t} \quad \text{(d)} \quad (12)$$

The equation that constitutes the excitation signal of a transducer is given as follows:

$$E(t) = G_1(t)e^{j2\pi f_0 t} + G_2(t)e^{j2\pi f_0 t} \quad (13)$$

It comes down to the exploitation of Equation 12a and b. If the medium of thickness d is characterized by a pulse response M (t, d), that means reflectors in this medium are aligned in the propagation axis of the ultrasonic beam then, the impulse response of a reflector situated at a distance d_i is a Delta function as shown by the following Equation 14.

$$M(t, d_i) = k(d_i)\delta\left(t - \frac{d_i}{c}\right) \quad (14)$$

Here K is a function of the depth considering the acoustic diffraction and the attenuation of the medium, and C is the ultrasound speed. Considering that impulse responses are short, the reflection function of the medium will be the sum of impulse responses for all depths. The echo signal R_x (t) will then be the sum of the convolution of the reflection function with the excitation signal.

$$R_x(t) = T_{x1}(t) * M(t, d_i) + T_{x2}(t) * M(t, d_i) \quad (15)$$

Equation 15 is nothing other than the time shift of the transmitted signal.

$$R_x(t) = \left(G_1(1-\tau_0) + G_2(1-\tau_0)\right)k e^{j2\pi f_0(t-\tau_0)} \quad (16)$$

$\tau_0 = d_i/C$ is a one way time of fly, corresponding to the beginning of the reception of the echo (Misaridis and Jongen, 2005; Jin et al., 2010). Since the simulation is at fixed frequency, there is no frequency dependency, and that is why after this step, the adapted filtering will be performed directly.

Adapted filtering is a process that allows the optimal detection of a signal present in an observation. Practically it is to get the signal out of the noise. To do so, it is necessary to know a minimum of information on the properties of the disturbing noise (Daffala et al., 2018) To perform the adapted filtering, the echo of the relation (16) was convolved with the expressions (12c) and (12d) and obtain the following relations S1(t) and S2(t):

$$S_1(t) = T'_1(t) * R_x(t)$$
$$= G'_1(t)e^{-j2\pi f_0 t} * \left(G_1(1-\tau_0) + G_2(1-\tau_0)\right)k e^{j2\pi f_0(t-\tau_0)} \quad (17)$$

$$S_2(t) = T'_2(t) * R_x(t)$$
$$= G'_2(t)e^{-j2\pi f_0 t} * \left(G_1(1-\tau_0) + G_2(1-\tau_0)\right)k e^{j2\pi f_0(t-\tau_0)} \quad (18)$$

Equation 19 is the sum of Equations 17 and 18 and it is the autocorrelation function, after realizing the adapted filter of the echoes.

$$RF(t) = \left[G'_1(t)e^{-j2\pi f_0 t} * \left(G_1(1-\tau_0) + G_2(1-\tau_0)\right)k e^{j2\pi f_0(t-\tau_0)}\right] + \left[G'_2(t)e^{-j2\pi f_0 t} * \left(G_1(1-\tau_0) + G_2(1-\tau_0)\right)k e^{j2\pi f_0(t-\tau_0)}\right] \quad (19)$$

According to the literature (Jin et al., 2010), $G'_1(t) * G_2(t-\tau_0) + G'_2(t) * G_1(t-\tau_0) = 0$.

Equation 19 then becomes:

$$RF(t)=\left[G_1^{'}(t)e^{-j2\pi f_0 t}*G_1(1-\tau_0)ke^{j2\pi f_0(t-\tau_0)}\right]+\left[G_2^{'}(t)e^{-j2\pi f_0 t}*G_2(1-\tau_0)ke^{j2\pi f_0(t-\tau_0)}\right] \quad (20)$$

Equation (20) is the simplified autocorrelation function and it representation will concerned only the real part as presented in Equation 21:

$$RF_{pic}(t)=R_e\left[G_1^{'}(t)e^{-j2\pi f_0 t}*G_1(1-\tau_0)ke^{j2\pi f_0(t-\tau_0)}\right]+R_e\left[G_2^{'}(t)e^{-j2\pi f_0 t}*G_2(1-\tau_0)ke^{j2\pi f_0(t-\tau_0)}\right] \quad (21)$$

RESULTS AND DISCUSSION

Bloc diagram of the characterization

To generate the two sequences of the 16 bits of the Golay code named Golay A and Golay B, two S-function was used and a program in the corresponding subsystem (subsystem sequence Golay A in addition to subsystem sequence Golay B respectively) put any bit at the same frequency as the nominal frequency and proceed to the BPSK modulation. It has been selected in these experiments, one cycle of the nominal frequency per bit of the Golay code. The pulse width of any bit is equal to one period of the high frequency, and that is the reason the phase changing at different bits in the graphs bellow can be observed. The simulation duration in Simulink/Matlab environment is 16 times the duration of 125 MHz frequency. Using the mathematical expression of Equations 19 and 20, the match filtering were performed after acquiring the reflected signals. To do so, the temporal returns of any previous signal were realized as follows. The phase of the high frequency was shifted from zero to 180° and flip different sequences of Golay code. As previously, the BPSK modulation of these new sequences is performing in subsystem sequence Inv Golay A, and subsystem sequence Inv Golay B. After the interaction with the medium model by attenuation coefficient of Honey containing pollen, the delay due to pollen size and a White Gaussian Noise with SNR equal to 5dB, the match filter is realized by the convolution of each reflected signal and the corresponding temporal return. The addition of the two match filtered signals gives the autocorrelation function.

Evaluation of attenuation coefficient of honey and pollen

The application of the experiment realized by Laux et al. (2011) in Equations 4, 5 and 6 gives the attenuation coefficient of honey and pollen in the considering thickness of honey as reported in the following Table 1. At 13.5 MHz, the attenuation coefficient of honey containing pollen (α_{mp}) is the sum of two attenuations coefficients and it is equal to $1.463*10^{-2}$ dB/µm/MHz$^{(\gamma=1)}$. The attenuation coefficient of honey containing pollen at 125 Mhz is calculated in agreement with the Equation 7. The result of the calculation of this parameter equal to 0.135 dB/µm/MHz$^{(\gamma=1)}$, considering that α_1 is equal to $1.083*10^{-3}$ dB/µm/MHz^2. This 125 MHz frequency is the one sized up at the beginning of this study when taking the option of encode signal for the characterization of honey containing pollen. As reported in Table 2, the attenuation coefficient of honey containing pollen for different values of power factor.

Signals obtain at different stages of the simulation

According to the simulation bloc diagram of Figure 2, the first interesting graphs are the BPSK modulation of 125 MHz with 16 bits Golay code and the temporal return of each of them. After the interaction of the signals in Figure 3 with the medium, the following Figure 5 is obtained. Figure 5 is the echoes signals obtained after applying the attenuation coefficient, the 400 µm delay, and a White Gaussian Noise with SNR equals to 5 dB. The autocorrelation function is obtained by convolution of each echo with the corresponding temporal return in Figure 4. Results are as follow in Figure 6.

The work proceed, in the same way, for different values of attenuation coefficient and considering the sample size (delay) as it is shown on the obtained results in Figure 7. As indicated in Table 2, the greater the power-factor, the greater the attenuation coefficient. In Figures 7d, e and f, the impact is more significant. To evaluate PSL and W_d, we get very close to the interesting portion as presented in Figure 7 (all the right figures). All the parameters are summarized in Table 3.

DISCUSSION

In Figure 3 the changing of phase depends on the bits applied. There is exactly 16 phases corresponding to 16 bits of the choosing Golay code. These signals are the same obtained by Nowicki et al. (2007) and Trots et al. (2011). Figure 4 is the reverse of Figure 3 and it is in accordance with the previous authors. However, one can observe a delay of about 4 µm due to the temporal return of Golay sequences. This undesirable delay will appear in autocorrelation function and can contribute to increase the dead zone that naturally exist in front of the transducer during it operation. According to Trots et al.

Table 1. Summary of acoustics parameters of the honey and the pollen and the evaluation of attenuation coefficient, α_m or α_p (dB/µm/MHz$^{(\gamma=1)}$), at 13.5 MHz.

For honey						
C_1(m/s)	**ρ_1 (kg/m^3)**	**R_{MPs}**	**A_i (V)**	**A_{MPs} (mV)**	**D (µm)**	**α_m (dB/µm/MHz)**
2030	1420	0.0409	200	150	150	**8.579*10^{-3}**
For pollen						
C_2(m/s)	**ρ_2 (kg/m^3)**	**R_{PiM}**	**A_{MPs} (mV)**	**A_{PiM} (µV)**	**D (µm)**	**α_P (dB/µm/MHz)**
1570	1218	0.0409	150	75	400	**6.047*10^{-3}**

Table 2. Attenuation coefficient of honey containing pollen at 125 MHz for different values of power factor **γ.**

Power factor (γ)	0.5	1	1.25	1.5	1.75	2
A_{mp}(dB/µm/MHz$^{\gamma}$)	0.012	0.135	0.451	1.509	5.047	16.875

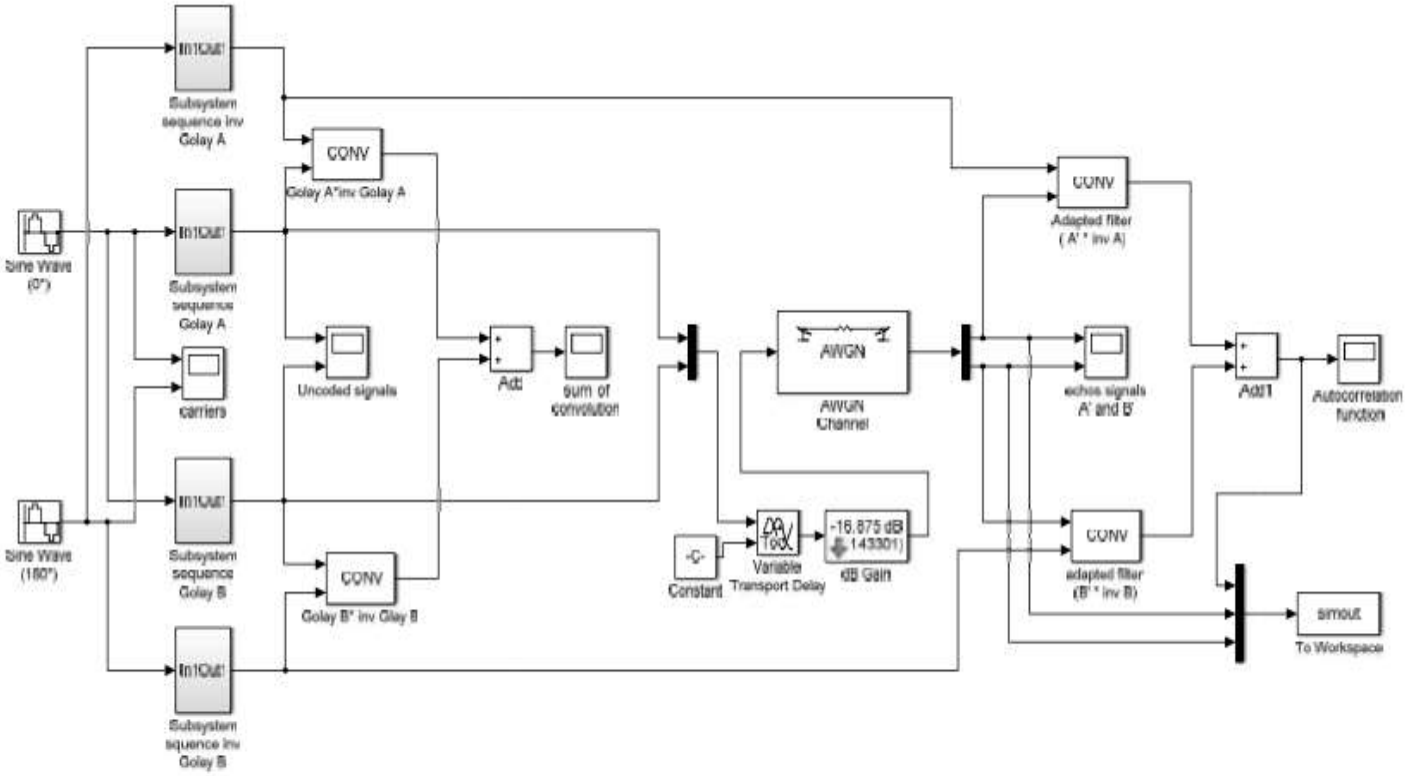

Figure 2. Block diagram for the evaluation of the impact of attenuation coefficient of honey containing pollen on BPSK signals at 125 MHz and realization of adapter filter.

(2008), the dead zone is due to the elongation of Golay code (Trots et al., 2008). It appears in this study that this elongation is not the only reason.

The width of the autocorrelation function decreases with the attenuation coefficient. This value specifies the range resolution of the signal. The PSL increases with the rising of attenuation coefficient. In literature, the side lobe-main lobe ratio of 16 bits Golay code is -21.0721 dB (Kabakchiev et al., 2010) and -24.08 dB (Sethi, 2013). The values obtained show losses of bits in the application. These losses increase with the attenuation coefficient of honey containing pollen and the application of AWGN.

In Figure 7, the power factor has a considerable impact on the determination of attenuation coefficient so is the transmission of characteristic signal. This power factor

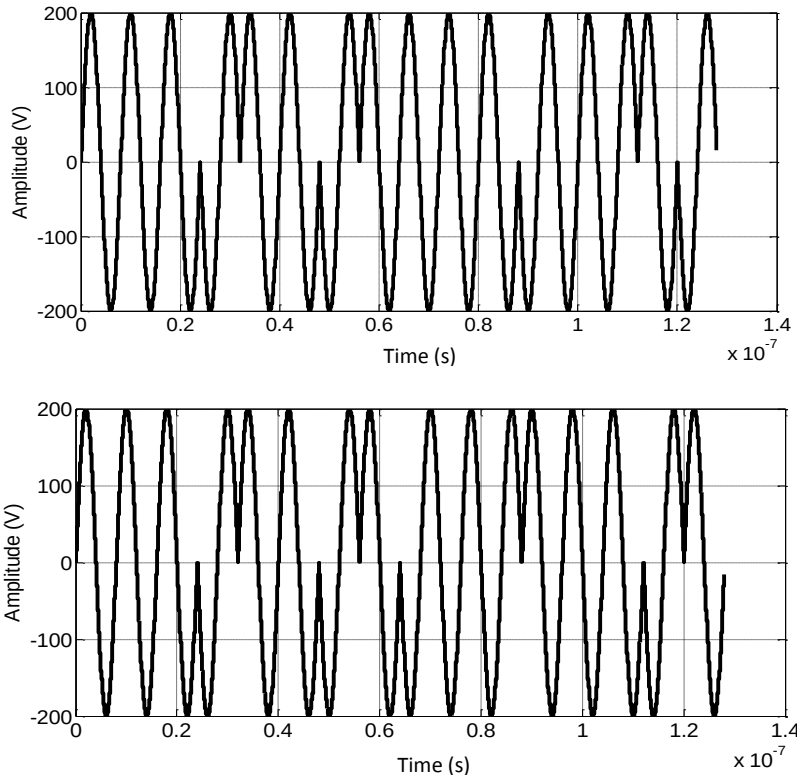

Figure 3. Encoded of 125 MHz signal with 16 bits Golay code A (up) and Golay code B (down) at 200V magnitudes.

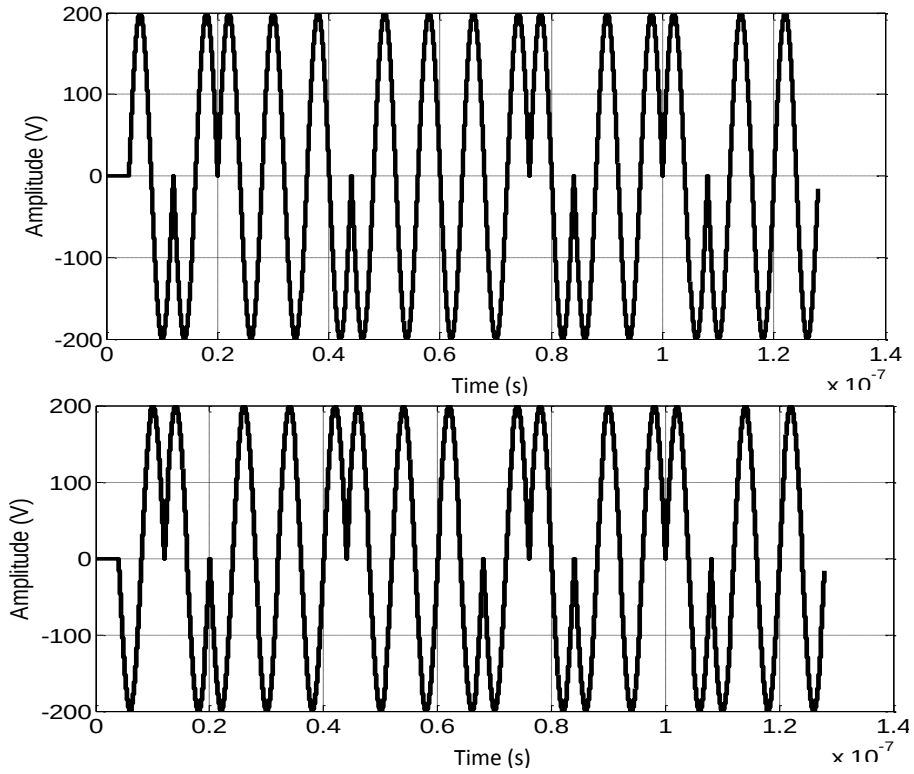

Figure 4. Temporal return of encoded signals at 125MHz with 16-bits Golay code A (up) and Golay code B (down).

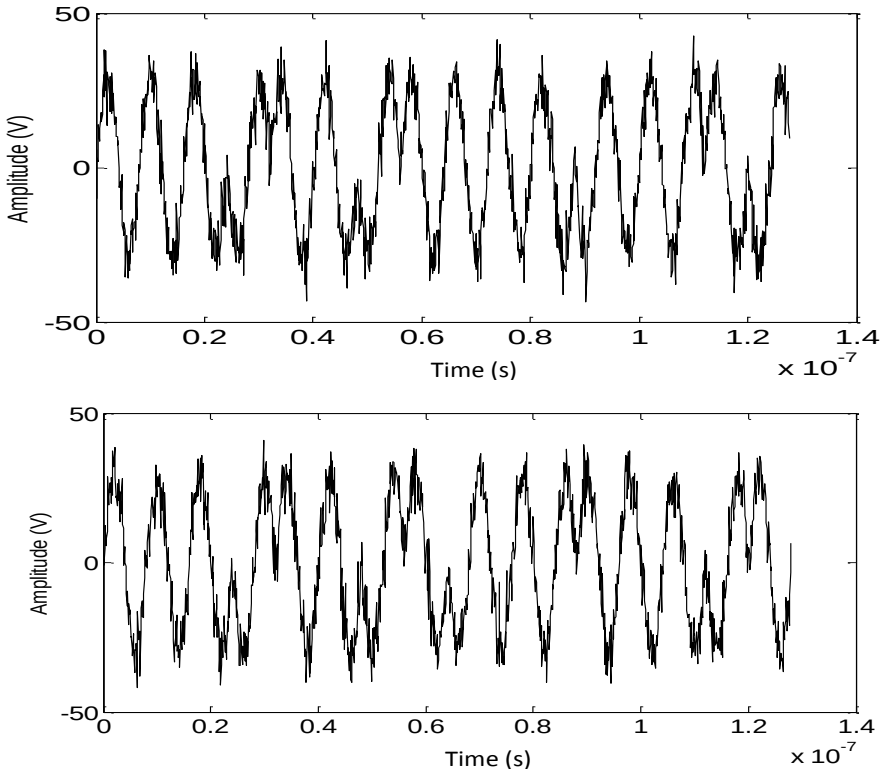

Figure 5. Echoes signals after undergoing the delay (400 μm) due to the pollen interface and the attenuation coefficient (16.875 dB/μm/MHz) of honey containing pollen.

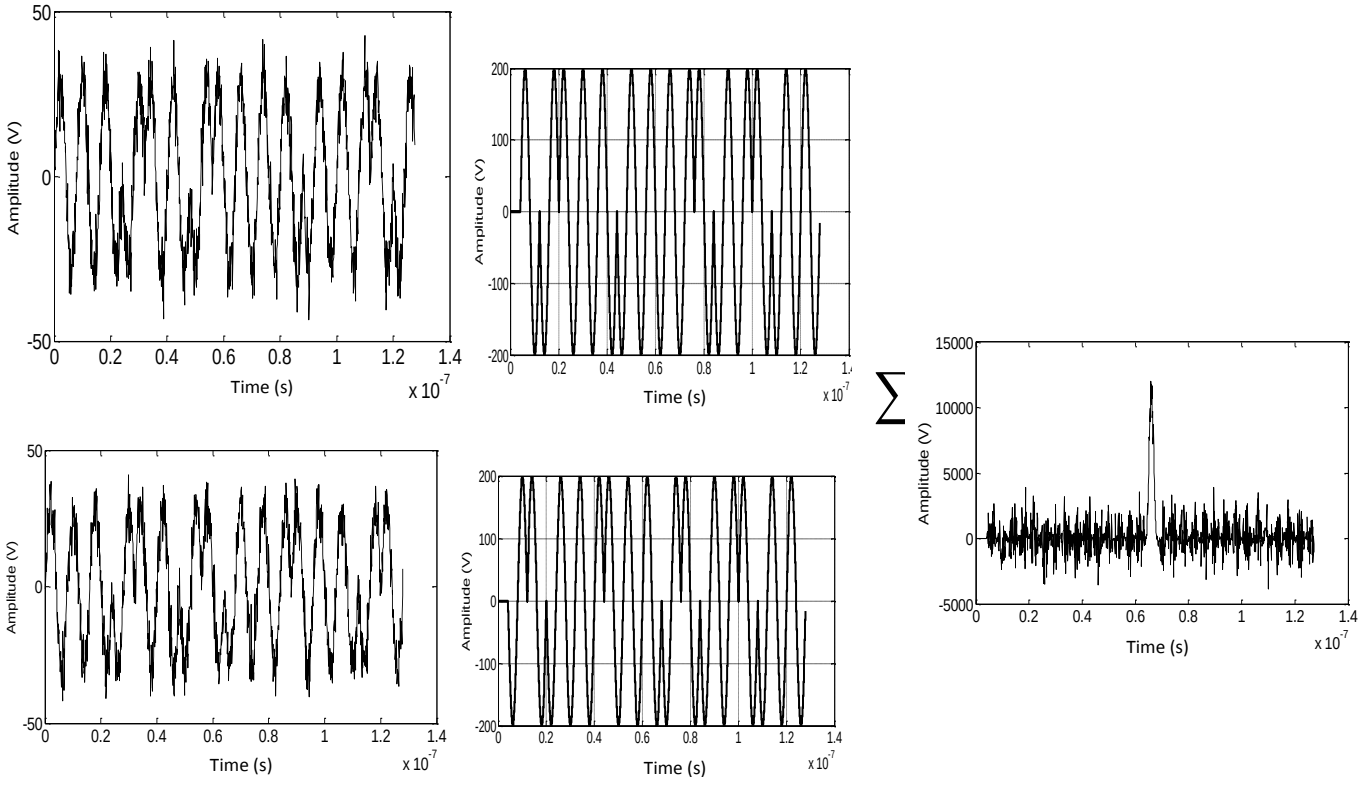

Figure 6. Autocorrelation function obtained after adapted filter realized with echoes signals and the corresponding temporal return (α=16.875 dB/μm/MHz, d=400 μm).

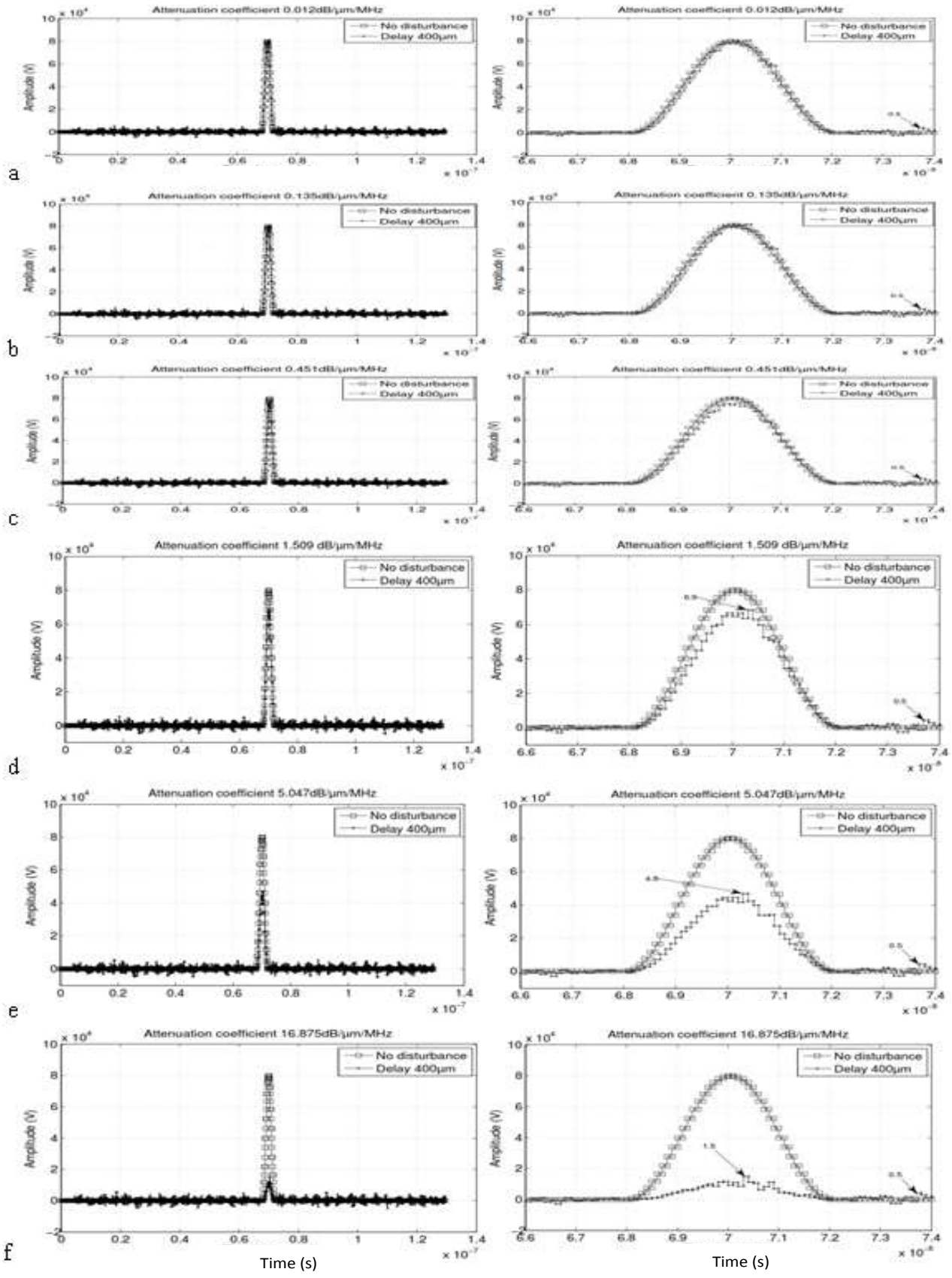

Figure 7. The autocorrelation functions at different values of attenuation coefficient and the delay (all columns in the left) the zoom in an interesting portion (all columns in the right).

Table 3. Summary of the evaluated parameters in the autocorrelation functions of the selected figures.

A (dB/µm/MHz)	Highest sidelobe amplitude (V)	Mainlobe amplitude (V)	PSL (dB)	Wd(ns)
Figure 7d: 1.509 (γ=1.5)	$5*10^3$	$69*10^3$	- 22.79	Rise time 68; Fail time 72; Wd = ~4
Figure 7e: 5.047 (γ=1.75)	$5*10^3$	$48*10^3$	- 19.45	Rise time 68.2; Fail time 72; Wd= ~3.8
Figure 7f: 16.875 (γ=2)	$5*10^3$	$15*10^3$	- 9.54	Rise time 68.3; Fail time 71.8;Wd= ~3.5

reveals the dispersion of the given honey. If the dispersion is high, attenuation coefficient of honey is high also. Cereser and Laux (2010b) found at 5 MHz that the attenuation coefficient of honey is around 30 µm (Cereser and Laux, 2010b). This result does not give any idea about the dimension of the attenuation coefficient of honey as was done in this work. Moreover, the operational frequency is 25 times theirs.

CONCLUSION AND RECOMMENDATIONS

This work valuated the attenuation coefficient of honey containing pollen and the work proceeded to the characterization of BPSK modulation of 16 bits Golay code at 125 MHz in Simulink/Matlab environment. The results have shown that the impact of attenuation coefficient of honey containing pollen on characteristics signals depended on the power factor that reveal the dispersion of the structure. The magnitude of the autocorrelation function is noticeable and can help to predict the behavior of BPSK signal in honey structure. The interest of this work is a contribution to recognise natural honey, doing so by the interpretation of a quantitative analysis of a sample. The lack of the consideration of the natural presence of the pollen inside of the honey, make us miss to study rightfully honey as a complex that possesses various interfaces. In future works, it would be interesting to study the effect of the composition of honey and moisture content on the attenuation coefficient. The implementation of this method of characterization will be carried out to construct a prototype and therefore to contribute to the rightful labeling of honey, taking into consideration the presence of pollen in it.

CONFLICT OF INTERESTS

The authors have not declared any conflict of interests.

ACKNOWLEDGEMENTS

The authors thank the anonymous reviewers for their valuable comments and suggestions to improve the quality of this paper. They are greatly indebted to the Cameroon Government for funding the research through the Ministry of higher education program “Modernisation de la Recherche dans l’Enseignement Supérieur”.

REFERENCES

Alvaro H, Urena J, Mazo M, Garcia JJ, Jemenez A, Alvarez FJ (2007). Reduction of blind zone in ultrasonic transmitter/receiver transducer. Sensors and Actuators A 133:96-103.

Alejos AV, Dawood M, Habeeb Ur RM, Sanchez MG, Jedlicka RP, Cuinas I (2008). Low Sidelobe Level Radar Techniques Using Golay Based coded Sequences. IEEE 978-1:4244-2042.

Aouzale N, Chitnalah A, Jakjoud H (2010). Utilisation d’une technique ultrasonore pour le contrôle de la qualité des huiles alimentaires, 10ème Congrès Français d’acoustique,<hal-00554461>.

Awad TS, Moharram HA, Shaltout OE, Asker D, Youssef MM (2012). Applications of ultrasound in analysis, processing and quality control of food: A review. Food Research International 48:410-427.

Berger G, Laugier P (1992). Intérêt et méthodologie de l’échographie quantitative. Journal de Physique IV 2:27-40.

Berson M, Feuillard G, Diridollou S, Letiecq M, Pourcelot L (1994). Imagerie ultrasonore haute résolution. Journal de Physique IV. C5:1285-1288.

Cereser CV, Laux D (2010a). Moisture content in honey determination with a shear ultrasonic reflectometer. Journal of Food Engineering 96:93-96.

Cereser CV, Laux D (2010b). High frequency shear ultrasonic properties of water/sorbitol solutions. Ultrasonics 50:6-8.

Chandrapala J (2015). Low intensity ultrasound application on food systems. International Food Research Journal 22(3):888-895.

Clair B, Despaux G, Chanson B, Thibaut B (2000). Utilisation de la microscopie acoustique pour l’étude des propriétés locales du bois: Etude préliminaire de paramètres expérimentaux. Annals of Forest Science 57:335-343.

Daffala MM, Babiker Awad A (2018). Adaptive coding, modulation and filtering of Radar signals. IntechOpen, Topic in Radar signal Processing pp. 213-241.

Duclos A, Ollivier S, Blanc-Benon PH, Mardsen O, Gilles B, Lafon C, Bera JC (2009). Modélisation de la propagation d’ultrasons non focalisés dans des gels de protéines, 10ème Congrès Français d’acoustique , <hal-00546817>.

Duclos A, Ollivier S, Lafon C, Bera JC, Gilles B, Blanc-Benon PH (2010). Propagation ultrasonore dans des gels modélisant les tissus biologiques, 19ème Congrès Français de Mécanique. http://hdl.handle.net/2042/36607.

Dahdouh S (2011). Filtering, Segmentation and follow-up of echographics images: clinical applications. Ph.D. Thesis, university of Paris sud XI. Original paper in French.

Edgar JB, Juluis OS (2008). Transfer Function Measurement Toolbox. https://ccrma.stanford.edu/realsimple/imp_meas/imp_meas.pdf.

Ferrus C (2012). Qualité des produits de la ruche. International workshop on the consequences of the ECJ judgment on GM pollen in honey for GM crop releases and cultivation in Germany and the EU, ITSAP, 12p.

Jin C, Chen SP, Qin ZD, Wang TF (2010). A new scheme of code ultrasound using Golay codes. Journal of Zhejiang University, Science C (Computers and Electronics) 11(6):476-480.

Kabakchiev A, Kyovtorov V, Barislov B, Kabakchiev C, Lazarov A

(2010). Numerical Analysis of different Communication Signals Used in Passive Radad Systems. Cybernetics and Information Technologies 10(4):75-90.
Kulmyrzaev A, McClements DJ (2000). High frequency dynamic shear rheology of honey. Journal of Food Engineering 45:219-244.
Laux D, Cereser Camara V, Rosenkrantz E (2011). α-relaxation in honey study versus moisture content: high frequency ultrasonic investigation, around room temperature. Journal of Food Engineering 103:165-169.
McClements DJ, Fairley P (1991). Ultrasonic Pulse Echo Reflectometer. Ultrasonics 29:58-62.
McClements DJ, Fairley P., (1992). Frequency Scanning Ultrasonic Pulse Echo Reflectometer. Ultrasonics 30(6):403-405.
McClements DJ, Sundaram G (1997). Ultrasonic Characterization of Foods and Drinks: Principlces, Methods, and Application. Critical Reviews of Food Science and Nutrition 37(1):1-46.
Mehryar L, Esmaiili M, Hassanzadeh A (2013). Evaluation of some physicochemical and rheological properties of Iranian honeys and the effect of temperature on its viscosity. American-Eurasian Journal of Agriculture and Environmental Science 86(2):981-994.
Misaridis XT, Morten HP, Jongen AJ (2000). Clinical use and Evaluation of Coded Excitation in B-mode Images. Ultrasonics Symposium pp. 1689-1693.
Misaridis XT, Jongen AJ (2005). Use of Modulated Excitation Signals in Medical Ultrasound. Part I: Basic concepts and Expected benefits. Transactions on Ultrasonics ferroelectrics and Frequency Control 52(2):171-191.
Nowicki A, Litniewski J, Secomski W, Lewin PA, Trots I (2003). Estimation of Ultrasonic attenuation in a bone using coded Excitation. Ultrasonics 41:615-621.
Nowicki A, Trots I, Lewin PA, Secomski W, Tymkiewicz R (2007). Influence of the ultrasound transducer bandwidth on selection of the complementary Golay bit code length. Ultrasonics 47:64-73.
Sethi S (2013). Optimal Selection of Binary codes for Pulse Compression in Surveillance Radar. International Journal of Engineering Research and Applications 3(2):216-223.
Shin OS, Kung HT, Tarokh V (2008). Construction of block orthogonal Golay sequences and application to channel estimation of MIMO-OFDM systems. Transactions on Communications 56 (1):27-31.
Sosnoskie LM, Webster TM, Dales D, Rains GC, Grey TL, Culpepper AS (2009). Pollen grain size, density and settling velocity for Palmer Amaranth « Amaranthus palmeri ». Weed Science Society of America 57(6):404-409.
Szabo TL (2014). Diagnostic Ultrasound Imaging: Inside Out. Academic Press 801 p.
Trots I, Nowicki A, Lewandowski M, Secomski W, Litniewski J (2008). Double Pulse Transmission-Signal to Noise Ratio Improvement in Ultrasound Imaging. Archives of Acoustics 33(4):593-601.
Trots I, Tasinkevych Y, Nowicki A, Lewandowski M (2011). Golay Coded Sequences in Synthetic Aperture Imaging Systems. Archives of Acoustics 36(4):913-926.
Vijay RK (2011). Side lobe Suppression Techniques for Polyphase codes in Radar. Master Thesis, National Institute of Technology, Roukela, India, P. 94.

Vol. 12(1), pp. 12-23, July-December 2020
DOI: 10.5897/JETR2020.0691
Article Number: BD8858E64487
ISSN: 2006-9790

http://www.academicjournals.org/JETR

Journal of Engineering and Technology Research

Full Length Research Paper

Modeling and experimental validation of drying processus of the microalgue Spirulina with consideration deformation and flow mass

E. Salmwendé Tiendrebeogo[1,2,3*], G. Christian Tubreoumya[1], A. Oumar Dissa[1], A. Compaoré[1], J. Koulidiati[1], F. Cherblanc[2], A. Bere[1] and I. Youm[3]

[1]Laboratoire de Physique et de Chimie de l'Environnement (LPCE), Université Joseph KI - ZERBO, 03 BP 7021 Ouagadougou 03, Burkina Faso.
[2]Laboratoire de Mécanique et Génie Civil (LMGC), CNRS, Université de Montpellier 2, Place Eugène Bataillon 34000 Montpellier, France.
[3]Centre de Recherche sur les Energies Renouvelables (CERER), Université Cheick Anta Diop, Dakar, Sénégal.

Recieved 21 April, 2020 ; Accepted 15 June, 2020

The profiles of the material transfer properties in porous products such as Spirulina platensis during drying which characterize their behavior are often determined from different experimental points by destruction of the samples. However, for a long drying time, it's impossible to slice or cut the sample correctly because of its mechanical strength and friability. It influences the evaluation of product in cylindrical form properties during all periods of drying. The study aim to propose a model to determine the evolution of water parameters of the micro-alga Spirulina platensis during an isothermal drying. A diffusive model taking into account the deformation and the mass flow of the product is proposed. The digital resolution and the experimental measurements over a period of 120 h of drying have shown a variation of water content (kg_w/kg_{dm}) of the order of 3.12 at 0.41 in the opposite direction of the product thickness and of flow ($kg_w/m^2.s$) in the order of 9.26 10^{-10} at 2.63 10^{-8}. The proposed model satisfactorily validates the experimental drying kinetics over all drying periods and the water content profiles for thicknesses less than 10 mm. The value of R^2 obtained is of the order of 0.980, indicating a good correlation between the experimental and predicted data; whereas the root mean square error is around 0.013, showing a very good match between experimental and modeled kinetics.

Key words: Modeling, experience, drying processus, properties evolution, microalgue spirulina, deformation.

INTRODUCTION

Local mass transfers in highly porous products such as spirulina platensis during drying translate or characterize elementary movements or behaviors that the mechanic wishes to represent and predict. It is therefore important

*Corresponding author. E-mail: tiendrebeogoeloi@yahoo.fr. Tel : (+226) 50 30 70 64/65.

to know how to understand them, interpret them, measure them and compare them. Experimental studies (Kieu et al., 2018; Dissa et al., 2014; Desmorieux et al., 2010) had already defined the first tracks on mechanical behavior and water properties. In porous media, some authors consider a transfer only in the liquid phase, while others differentiate free water from bound water and take into account the transport of matter in the gas phase (Ramirez-Martinez et al., 2013; Pinto and Tobinaga, 2006; Katekawa and Silva (2006). The diffusive term is classically expressed as a function of the gradient of water content or of the concentration governed by the Fick model, but it is sometimes described by Darcy's law which allows to consider the pressure gradient. It can also be a function of the temperature gradient and take into account the mechanical properties of the product such as the Young's modulus and the fish coefficient. If mass diffusion takes place only in the liquid phase within the product, the evaporation of water takes place only on the surface. The coexistence of these phases within the material cannot be excluded. The adsorption isotherm (Monsurat et al., 2019) and the drying kinetics provide information on the overall behavior of the food dough (Tiendrebeogo et al., 2019; NFX15-119, 1999; Kalika and Alam 2014). However, it is shown in these works that the mass flux is associated with the apparent density gradients of water. These variables were identified through profiles measured experimentally by the destructive method of samples (slicing). The profiles are reconstituted from various points of experimental measurements, whereas for a very long drying time it is impossible to slice or cut the sample correctly because of its mechanical strength and its friability. This does not allow us to know the evolution of the kinetic and water parameters during all the drying periods. The experimental procedure being complex, relatively long in the slicing limit of the material and validates only part of the drying process, a prediction of the evolution of the water content profiles by a diffusion model is essential to describe the water diffusion mechanism. It is in this context that the objective of this work was to estimate the evolution of the water parameters of the *Spirulina platensis* in space and time during an isothermal drying experimentally and by a model. It's about:

(i) to model taking into account the deformation and the mass flow;
(ii) to determine the mass flow and water content fields in *S. platensis* and their evolution in space and time;
(iii) experimentally validate the modeling results.

MATERIALS AND METHODS

Experimental procedure

Sampling

The material used in this study for the validation of the mathematical model is a sample *of S. platensis* from the exploitation site located in La Fon del Cardaire, a farm located in Gignac in the south of France. A pretreatment was carried out on the harvested biomass to eliminate a good part of the culture water until reaching a given water content. Thus, the water content is reduced to 3.12 kg_w/kg_{dm} by wringing under the action of vacuum. This water content obtained after pretreatment is considered to be the initial water content of the sample for the experiment. The initial characteristic parameters recorded in Table 1 had already been determined using standard methods (NFX15-119, 1999; Tiendrebeogo et al., 2015). After spinning, the fresh *S. platensis* is transformed into samples suitable for testing. A cylindrical shape commonly used in farms during drying is adopted. A design process is defined in order to avoid the variability of the samples: the fresh biomass is molded in a cylindrical form 20 mm in diameter and 40 mm thick using a piston extruder consisting of a cylindrical tube Teflon and a steel piston; the cylindrical lateral surfaces of the samples are wrapped with a plastic film of negligible mass to avoid adhesion between the sample and the support and to ensure one-dimensional transfer; samples with initial masses on the order of 13 g are selected for use during the experiments (Figure 1). It is assumed that these conditions are met and the samples are uniform in the initial state.

To understand experimentally the distribution of water in the product during drying, the study followed the variation of the water content in the product by cutting samples. The water content in a sample slice is determined by considering the mass of this slice at a given time and that of the solid phase according to the following Equation 1:

$$w = \frac{m(x,t) - m_s}{m_s} \quad (1)$$

Drying experiments

Cutting method: samples are put to dry in a desiccator whose temperature is regulated in the order of 50°C and de *HR* is 6% respectively by a brand oven Memmert UFP 600 (Figure 2) and a potassium hydroxide solution (KOH). At each instant t, one of the samples is taken and weighed with a precision electronic balance 10^{-3}. Then it was placed it in the cutting system (Figure 3) to transform it into slices 2 mm thick perpendicular to the axis $(\vec{ox})$ using a blade 0.25 mm. The slices are then placed in the oven maintained at 70°C for 48 h to obtain their dry mass. The average water content of a sample at a given time is obtained by calculating the average of the water contents of the wafers.

In order for the moisture content profiles sought to be characteristic of a given single sample, all the samples should be in the same state at the start of the process. Thus, they are prepared under the same conditions as indicated above. The material being symmetrical, the averages of water contents of the points symmetrical compared to the median plane are considered. This approach provides access to the water content profiles $w(x,t)$ corresponding to moments of drying. Since the study aimed to characterize the phenomena of water transport in a single sample from measurements obtained on various samples, it is essential to have the same initial conditions in all the samples. Even if particular attention is paid to the preparation of samples, this methodology may present some deviations. For this, the experimental water content profiles are approached by simple polynomial equations (Equation 2) introducing 3 constant parameters a, b and c at each time.

$$w(x,t) = ax^4 + bx^2 + c \quad (2)$$

Table 1. Initial characteristics of the material. (Salmwendé et al., 2015)

Parameter	Symbol and units	Sample
Solid apparent density	ρ_s [kg/m^3]	255
Water apparent density	ρ_w [kg/m^3]	799
Solid real density	ρ_s^* [kg/m^3]	1270
Ratio of real densities	α […/…]	0.787
Porosity	ϕ […/…]	0.799
Water content	w [kgw/kgdm]	3.120

Source: Tiendrebeogo et al. (2015).

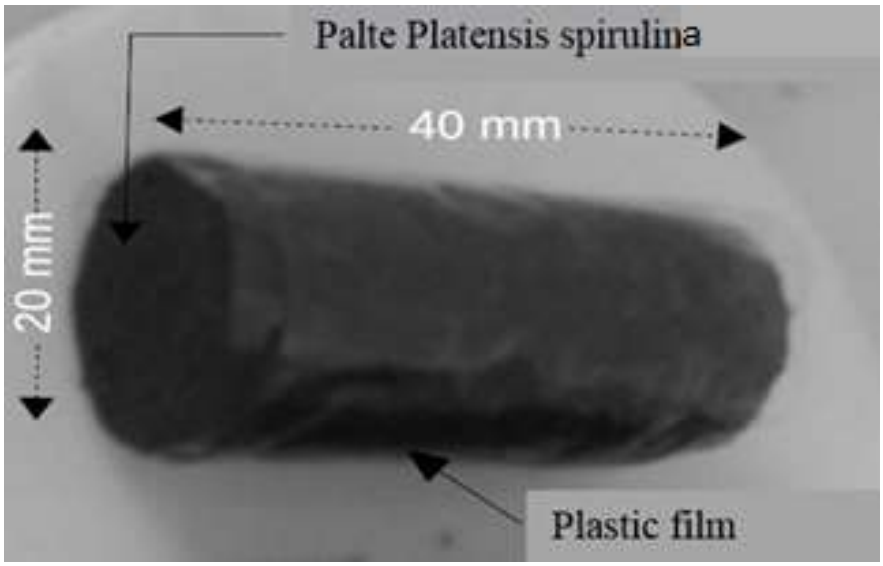

Figure 1. Study sample cylinder

Figure 2. Isothermal drying device.

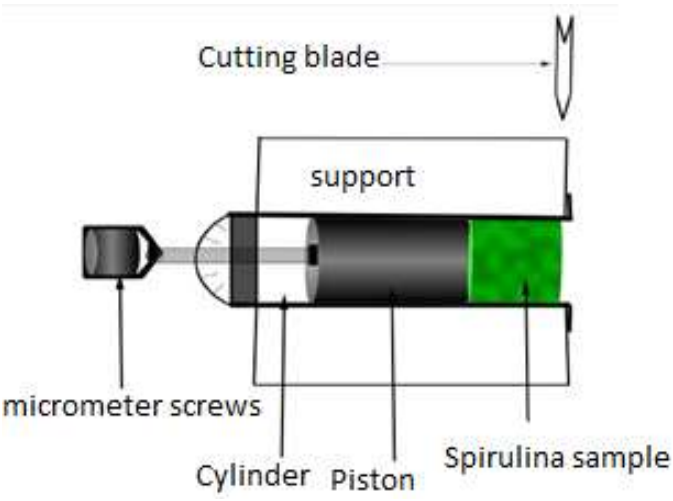

Figure 3. Device for cutting samples.

The tests were carried out at 50°C and lasted no more than 120 h (5 days). Because for a long drying period the material begins to stiffen and the cutting becomes delicate. For low temperatures (below 25°C) drying is very slow to reach values with low water content and the range of water content studied is too narrow. For too prolonged drying the material begins to denature and the development of microorganisms is observed. This could alter the water transport processes and should be avoided. Furthermore, the accuracy in the determination of experimental results estimated the statistical parameters: the coefficient R^2 and the root mean square error (RMSE). These parameters were expressed according to the following equations (Monsurat et al., 2019) which were solved by multi-linear regression analysis.

$$RMSE = \sqrt{\frac{\sum_{z=1}^{N}(Y_{\exp,z} - Y_{pre,z})^2}{\sum_{z=1}^{N}(\bar{Y}_{\exp,z} - Y_{pre,z})^2}} \quad (3)$$

$$R^2 = 1 - \frac{\sum_{z=1}^{N}(Y_{\exp,z} - Y_{pre,z})^2}{\sum_{z=1}^{N}(\bar{Y}_{\exp,z} - Y_{pre,z})^2} \quad (4)$$

MODELING

Physical configuration of model and Hypothesis

Concerning the numerical simulation, the drying conditions are the same as those of the experiment, the only difference is that one takes into account the axisymmetric geometry. That is to say the existing symmetry along the cylindrical axis ($\overrightarrow{ox}$) and the one following the median plane (the axis $\overrightarrow{oy}$) are considered (Figure 4). The simulation is done in a 2D rectangular geometry which considers only a quarter of the sample (Figure 5). The surfaces 4 and 1 respectively represent the planes of symmetries along x and y where the mass and heat fluxes are zero, as well as the surface 2 isolated with a plastic film. The surface 3 is supplied by a convective heat flow, heat flow by evaporation and an imposed mass flow which only crosses the exchange face (surface 3). The mass flow is absorbed by the air on this surface. The surface forces which could be added by the action of the film layer are negligible. For to be near to the characteristic aspects of the environment to be studied, simplifying theoretical hypotheses have been posed:

(i) the solid and liquid phases are assumed to be incompressible and the actual volume densities $\rho_w^* = cste$; $\rho_s^* = cste$ are constant.
(ii) the constitutive medium remains two-phase and modeled by a poro-elastic material.
(iii) material modeling is axisymmetric

Mass transfer equations

(i) Behavioral relationship

The filtration behavior of all fluids (liquid, vapor and gaseous) in the medium is written using the generalized DARCY law:

$$\vec{q}_{w/s} = -\frac{\bar{k}}{\mu_w}\vec{\nabla}P_w^* \quad (5)$$

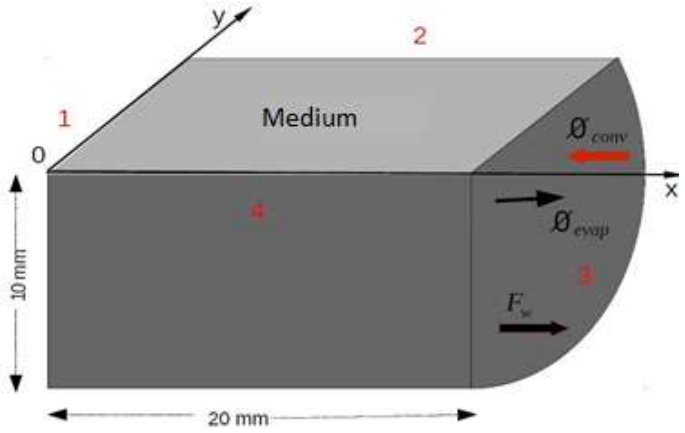

Figure 4. Quarter geometry of the sample considered for the simulation ($\varnothing_{conv}$ convective heat flow; $\varnothing_{evap}$ evaporative heat).

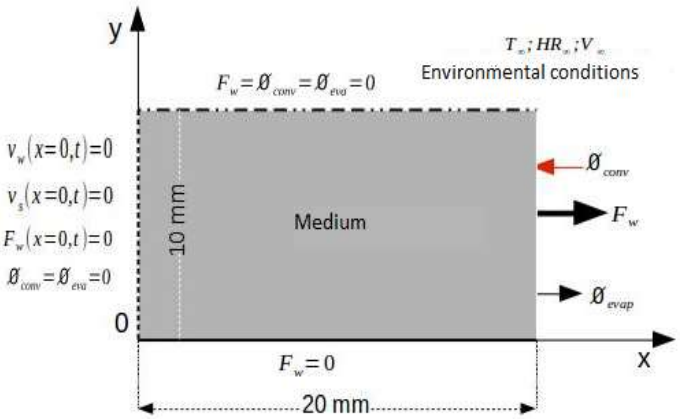

Figure 5. 2D schema of the drying conditions applied to the environment for the simulation.

The behavior of a poro-elastic material is considered:

$$\sigma_s = E\varepsilon - P_w^*\bar{\delta} \quad (6)$$

(i) Conservation equations

The formulation of the conservation equations is based on the various theoretical and experimental works developed for porous deformable and undeformable materials. For two-phase models, there is an equation for each phase (Equations 7 and 8). The liquid mass balance and solid balance equations are given respectively by Equations 3 and 4 (Anoua et al., 2014; Gowen et al., 2008).

$$\frac{\partial \rho_w}{\partial t} + \frac{\partial \rho_w u_w}{\partial x} = 0 \quad (7)$$

$$\frac{\partial \rho_s}{\partial t} + \frac{\partial \rho_s u_s}{\partial x} = 0 \quad (8)$$

The consolidation approach of an isotropic medium in linear

elasticity, developed by Marcelin Biot in 1941 was used (Seyied et al., 2015). The state parameters involved are: σ_s, ε, P_w^*. The generalized mass balance equation is given by:

$$\frac{1}{M}\frac{dP_w^*}{dt} + b\vec{\nabla}.\overrightarrow{u_s^*} = -\vec{\nabla}.\vec{q}_{w/s} \quad (9)$$

The sample to be studied being assimilated to an elastic two-phase medium, at equilibrium, the conservation of quantity is materialized:

$$\vec{\nabla}\sigma_s + b\vec{\nabla}P_w^* + \rho\vec{g} = \vec{0} \quad (10)$$

By taking Terzaghi's hypothesis (the real densities of the constituents remain constant), the Biot coefficient or the specific capacity is b = 1.0 and the compressibility coefficient is zero $\frac{1}{M} = 0$. For a medium supposed to be undeformable, the displacement of the solid can be considered zero. For this type of (isothermal) drying, the only nodal variables considered are: w and F_w. A number of hypothesis are made in addition to those previously identified:

(i) In the case of isothermal drying at low temperature, the pressure gradients are neglected.
(ii) There is only one motor gradient: water content.
(iii) The effect of gravity can be overlooked.
(iv) Evaporation of water takes place on the external surface of the medium.
(v) The compressibility effects of the gas are negligible.

Behavioral relations, Equations 7 and 8 becomes as follows:

$$\vec{\nabla}.(\overrightarrow{u_s^*} - \frac{\bar{k}}{\mu_w}\vec{\nabla}P_w^*) = 0 \quad (11)$$

$$\vec{\nabla}.E\varepsilon - \vec{\nabla}P_w^*\bar{\delta} = 0 \quad (12)$$

The water content conservation equation.

By defining the dry base water content as follows:

$$w = \frac{\rho_w}{\rho_s} \quad (13)$$

and replacing ρ_w in the liquid conservation equation (Equation 7), the study arrived at the equation below:

$$\rho_s\frac{\partial w}{\partial t} + \vec{\nabla}.(\rho_w^*\overrightarrow{u_w}) = 0 \quad (14)$$

The mass flow of evaporated water is defined by:

$$F_w = \rho_w(u_w - u_s) = \rho_w u_w - w\rho_s u_s = -D_w\frac{\partial\rho_w}{\partial x} \quad (15)$$

By applying the law of species conservation, it was deduced from Equation 15, the expression of the diffusive model in saturated medium (Justin et al., 2015; Dissa et al., 2014).

$$\frac{\partial\rho_w}{\partial t} - \vec{\nabla}.(D_w\vec{\nabla}.\rho_w) = 0 \quad (16)$$

D_w is the diffusion coefficient and it depends on the nature of the material but also on the hydrodynamic parameters. It is determined from experimental data and its evolution is materialized by the Equation 17 (Tiendrebeogo et al. 2015).

$$D_w = 2.7810^{-10} + 3.3310^{-12}\exp(3.12w) \quad (17)$$

Initial conditions and limits

At *t* =0, the initial conditions express the uniformity of the water content of the sample and the state of the mass flux at the exchange surface.

$$w = w_0 \text{ and } -D_w\vec{\nabla}.\rho_w\vec{n} = F_m = 0 \quad (18)$$

At a given time t, the condition at the level of the symmetry planes (median plane and plane along the cylindrical axis) and at the isolated surface of the product is the same:

$$-D_w\vec{\nabla}.\rho_w\vec{n} = F_m = 0 \quad (19)$$

The boundary condition associated with the exchange area is determined as follows:

$$-D_w\vec{\nabla}.\rho_w\vec{n} = F_m \quad (20)$$

F_m The mass flow imposes on the end (exchange surface) of the sample. It is represented by an exponential function resulting from a derivation of the approximate equation of drying kinetics, with L_m =0.02 m, half the length of the sample.

$F_m = \rho_w^*(a'b'\exp(-b't))\frac{\alpha}{(\alpha+w)^2}L_m$ with a' =1.885, b'= $5.948.10^{-6}$ and α the ratio of real densities is around 0.787.

Numerical resolution

For the resolution of the mathematical model, the LMGC90

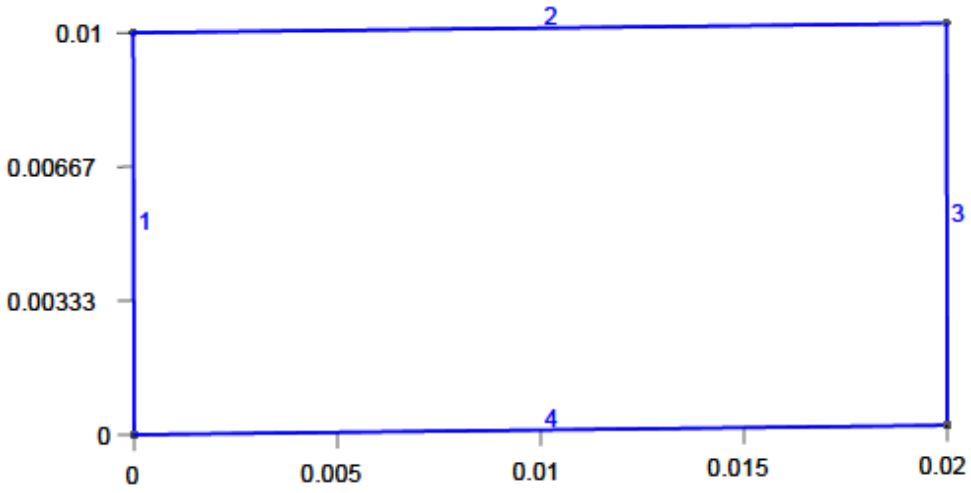

Figure 6. Sample geometry for simulation.

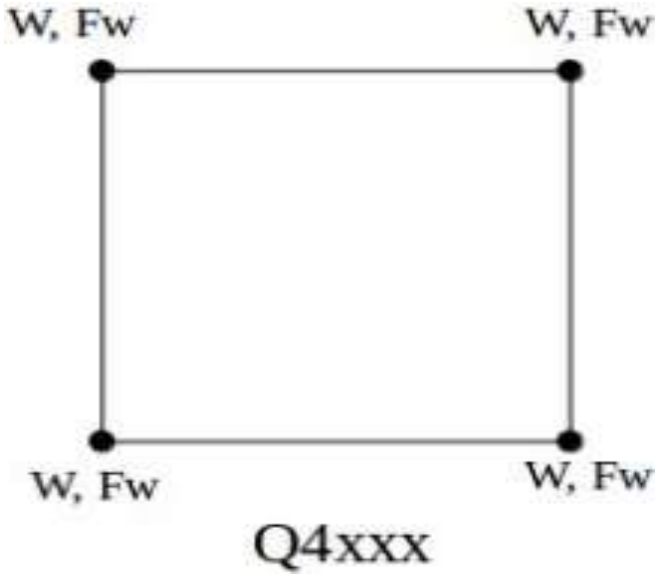

Figure 7. Mesh of elements Q4xxx.

calculation code was adopted, which takes into account all the requirements that the model requires for its numerical resolution.

Geometry of the sample

The geometric construction (Figure 6) of the sample model for the simulation is carried out in a python script defining the dimensions, shape and physical groups (end, axis, symmetry, surface).

Mesh of the model sample

Given the complexity of the model, a numerical resolution is essential and relates to the mass balance and transport equations. The method used is that of finite elements. The resolution of the finite element system amounts to meshing our material in Taylor-Hood elements (Figure 7) with well-defined nodes to carefully examine the dependence of w and the evolution of physical quantities. The problem is managed by a mesh in triangular elements (Q4xxx), order 1 with 231 nodes as shown in Figure 8.

RESULTS AND DISCUSSION

Numerical simulation

Water content and mass flux fields

Before tackling the quantitative prediction of the profile

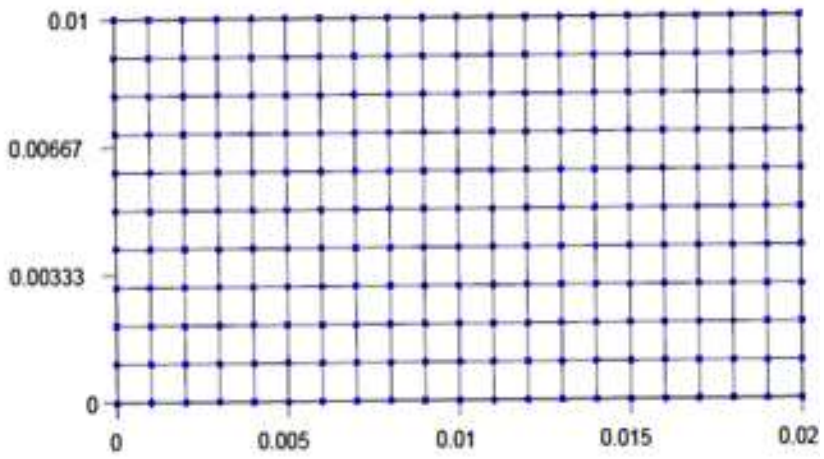

Figure 8. Sample mesh for simulation.

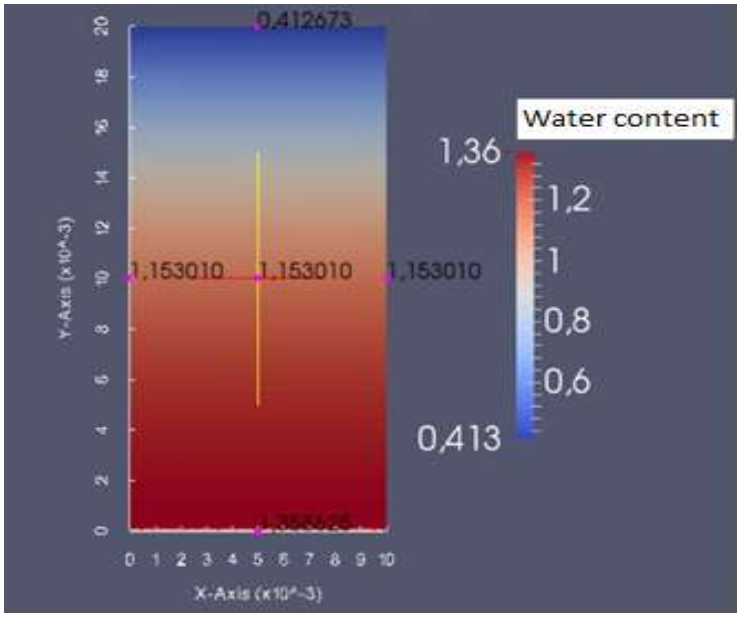

Figure 9. Simulated water content field (W_0 =3.12 kgw/kgdm).

field for different stages of exchange, it seems advisable to describe the availability of water and the evolution of mass flow during a simulation of diffusion carried out in the conditions indicated above. Figures 9 and 10 show the water content and linear density flux fields obtained after 102 h of drying a sample, respectively. In all cases, the entire sample is in the hygroscopic range with a color code expressed by the color blue for low values of quantities and the color red for high values. The analysis is based on the different colors and of course on the values taken at the reference time (120 h). Mass flows gradually settle towards the center of the product. The water content and flow in the sample vary differently, respectively on the order of 1.36 kg_w/kg_{dm} at 0.41 kg_w/kg_{dm} and in the order of 9.63 10^{-10} $kg_w/m^2.s$ at 2.2610^{-8} $kg_w/m^2.s$ This implies that the water transfer process in the product studied is governed by a single quantity: that is to say the water transport coefficient. As the drying is unidirectional, only the exchange surface dries first and has the lowest water contents. While that on the surface of symmetry, they reach 1.36 kg*w*/kg*dm*. The water content values recorded at points located on the physical groups: end, central axis, symmetry and isolated part, allow to draw only for a coast (*x)* given (thickness), the

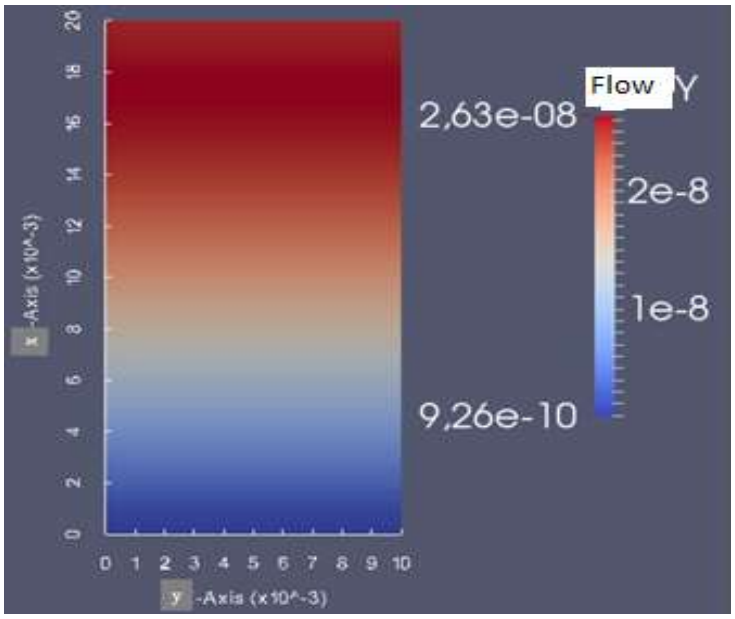

Figure 10. Champ de flux massique simulé.

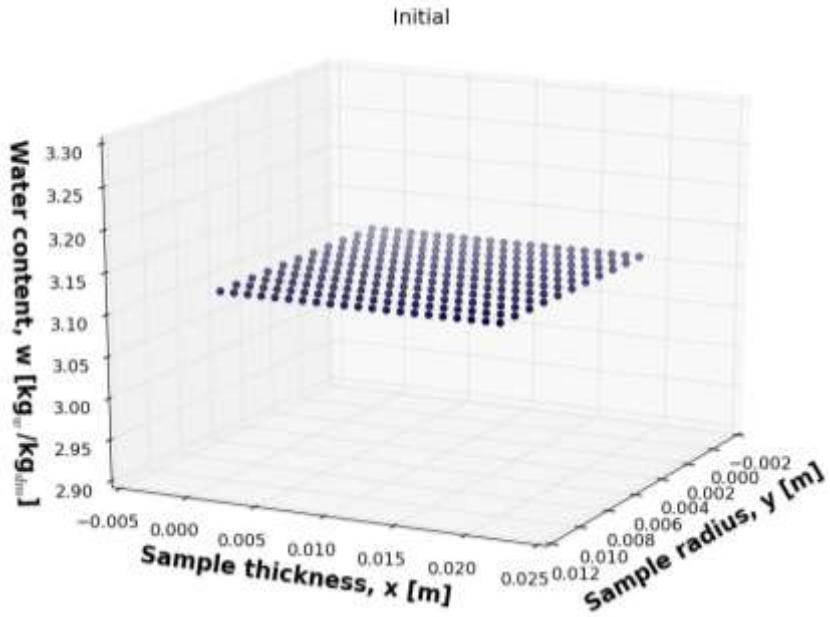

Figure 11. Fields of water content in *S. platensis* before drying (Initial state).

diffusion of water within *S. platensis* is uniform.

Evolution of spatial and temporal profiles of water content

Figures 11, 12, 13 and 14 show the spatial distribution of water within the *S. platensis* cylinder a homogeneous distribution within the product in the initial state can be clearly seen (Figure 5). From the start of the process, it becomes heterogeneous in the radial plane as well as in the axial plane and the upper surface dries faster than that of the plane of symmetry inside the product. The latter phenomenon was observed in an experimental study (Tiendrebeogo et al., 2015). Over time, the diffusion of water marks a short constant phase in the areas of the

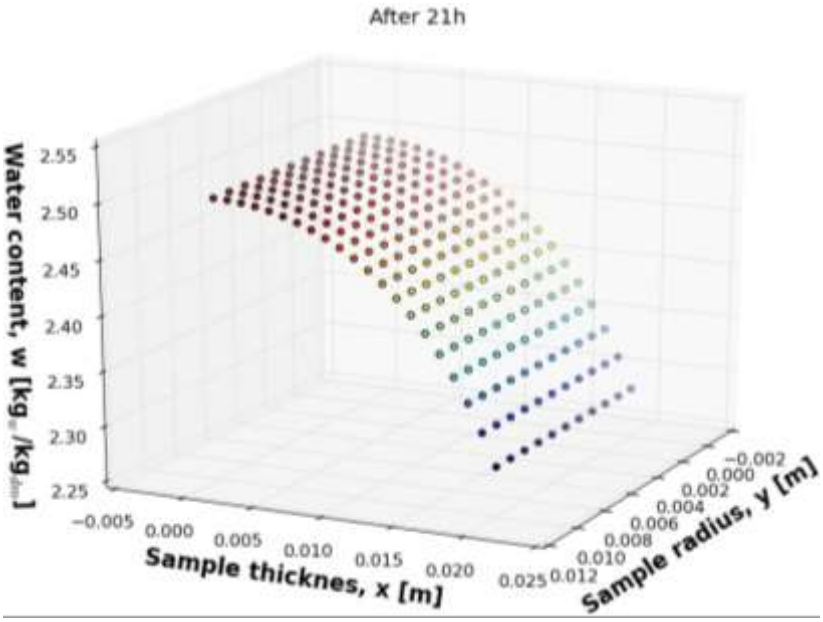

Figure 12. Fields of water content in *S. platensis* after 21 h of drying.

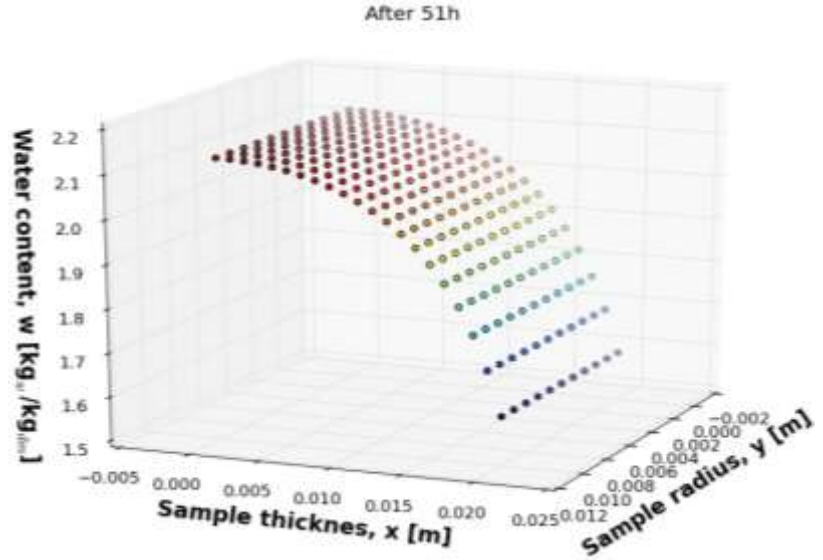

Figure 13. Fields of water content in *S. platensis* after 51 h.

sample near to its medium before going through a decreasing phase to tend towards a low water content, in this case the water content of balance. The surface exposed directly to the drying air reaches this equilibrium faster than the interior of the sample.

Experimental validation of model

The study validates the model by comparing the experimental results and those simulated. The distribution of the water content being uniform for a given thickness, the average of water content by thickness was considered to compare the results obtained by the digital method in this manuscript. The validation of the proposed model is carried out by comparing the kinetics (temporal evolution of the average water content of the product) from the numerical simulation (obtained using LMGC90) of the convective drying of Spirulina platensis, with those obtained experimentally. Indeed, this comparison shows

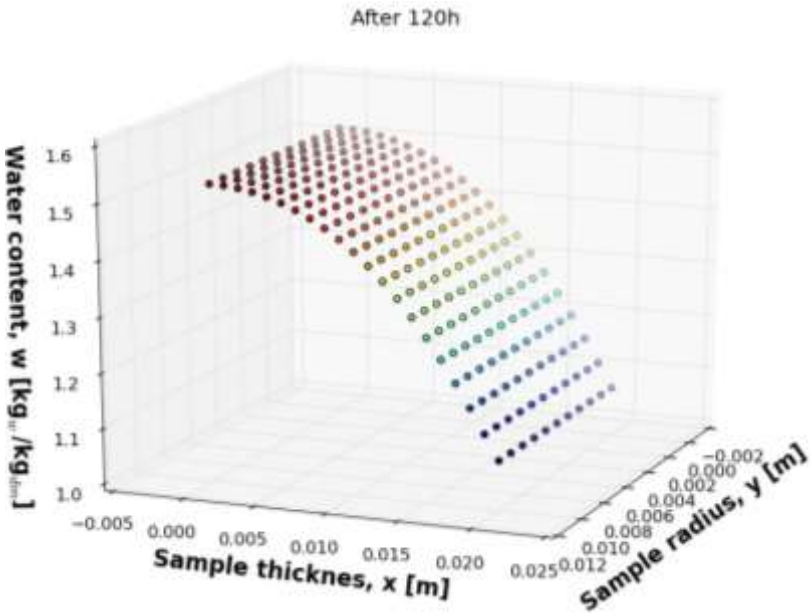

Figure 14. Water content fields in *S. platensis* at t = 120 h.

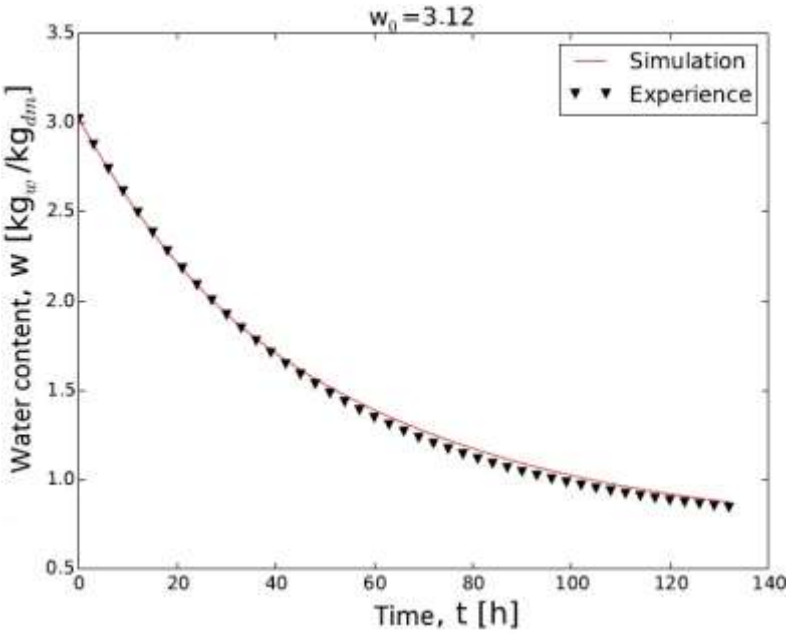

Figure 15. Comparison of simulated and experimental average water contents.

that the results of the numerical simulation are in agreement with those of the experiments (Figure 15 and Table 2). It can be observed that the proposed model is capable of predicting the drying kinetics. The differences observed between the experimental results and those obtained by the simulation can be qualified as minor. They may be due to the exact lack of knowledge of certain parameters. Another reason which can generate a gap between the experiment and the simulation, is the fact that our model concerns only a saturated medium.

Another comparison made between the experimental water content profiles and those simulated is shown in Figure 16. The simulation of the diffusion gives rise to specific curve shapes of the water content profiles and highlights the shrinkage of the solid. From the two graphs, it was noted that a concordance of the results for small thicknesses is towards the core of the material and large differences in the areas close to the exchange

Table 2. Water content and flux experimental and simulated.

	$0 \le x \le 20$		$0 \le x \le 10$		$0 \le x \le 5$	
	0 h		**120 h**		**120 h**	
	W	F_w	W	F_w	W	F_w
Experience	3.12	09.26×10^{-10}	0.70	2.63×10^{-8}	1.36	09.32×10^{-10}
Model	3.12	10.12×10^{-10}	0.80	2.05×10^{-8}	1.15	09.45×10^{-10}

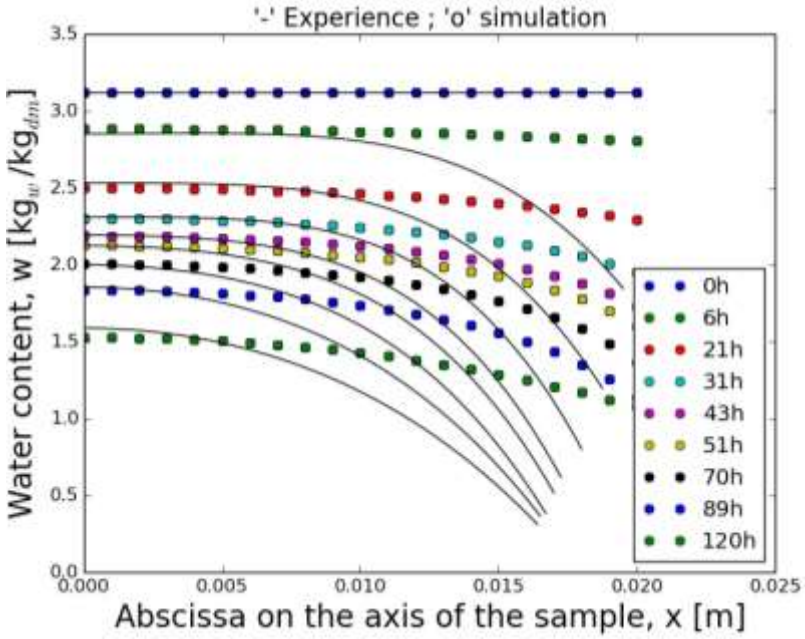

Figure 16. Comparison between the simulated profiles and those of the experience.

surface, that is to say for thicknesses greater than 10 mm. These profiles, which had been observed experimentally in 2016 (Tiendrebeogo et al., 2015), are more straightforward than those observed in coffee (Ramirez et al., 2014). The experimental results show that the contraction of the product is greater in the regions close to the surface. The fact that the shrinkage was not taken into account in the simulation could be at the origin of these observed divergences. The value of R^2 obtained is of the order of 0.980, indicating a good correlation between the experimental and predicted data; whereas the root mean square error (RMSE) is around 0.013, showing a very good match between experimental and modeled kinetics.

All the elements of comparison between simulation and experience have shown that the proposed model makes it possible to reproduce and write satisfactorily the evolution of drying kinetics throughout drying. And the water content profiles for any thickness less than 10 mm. From these results, it is observed that the range of validity of the model deteriorates at the back of the drying periods when one moves away from the core of the product, that is to say for thicknesses greater than 10 mm. Indeed, the extreme variations of the parameters of the material such as the mechanical properties (Young's modulus, Poisson's ratio) during these periods modified its mechanical behavior.

Conclusion

In this article, it was a matter of mathematically modeling and experimentally validating the evolution of the water parameters of the micro-alga *S. platensis* during isothermal drying taking into account the deformation and the mass flow. The numerical resolution of the mass transfer equations by the finite element method in the LMGC90 code made it possible to know the fields of

water content and mass flow, to represent the simulated profiles and to validate the experimental results and to define the domain of validity of the model. A model taking into account the contraction of the solid could accurately write the diffusion of water in *S. platensis*.

CONFLICT OF INTERESTS

The authors have not declared any conflict of interest.

NOMENCLATURE

HR, relative humidity (%); dm, dry matter (kg_w/kg_{dm}); d, cylinder diameter (m); w, water content (kg/kg); t, time (s); D_w, transport coefficient (m^2/s); F_w, mass water flux ($kg.m^{-2}.s^{-1}$); G_w, gradient of water density (kg/m^4); m_{eq}, equilibrium mass of sample (kg); m_i, sample initial mass (kg); x, sample thickness (m); m_s, dry mass of sample (kg); u_s, velocity of the solid phase (m/s); u_w, velocity of the liquid phase (m/s); w_{eq} equilibrium moisture content (kg/kg); α, real densities ratio (%); ρ_s, solid apparent density (kg/m^3); ρ_w, water apparent density (kg/m^3); ρ_s^*, solid real density (kg/m^3); ρ_w^*, water real density (kg/m^3); ϕ, porosity (%); R^2, coefficient of determination and RMSE, root mean square error.

REFERENCES

Anoua M, Ramirez-Martinez A, Cherblanc F, Bénet JC (2014). The use of chemical potential to describe water transfer in complex media with strong solid-liquid bonding. Transport in Porous Media 102:111-122.

Desmorieux H, Madiouli J, Herraud C, Mouaziz H (2010). Effects of size and form of Arthrospira spirulina biomass on the shrinkage and porosity during drying. Journal of Food Engineering 100 :585-595.

Dissa A, Compaore A, Tiendrebeogo E, Koulidiati J (2014). An effective moisture diffusivity model deduced from experiment and numerical solution of mass transfer equations for a shrinkable drying slab of microalgae spirulina. Drying Technology 32:1231-1244.

Tiendrebeogo ES, Dissa AO, Cherblanc F, Youm I, Bénet JC, Compaoré A, Koulidiati J (2015). Characterization of Two Different Stumps of Spirulina platensis Drying: Assessment of Water Transport Coefficient. Food and Nutrition Sciences 6:1437-144. http://dx.doi.org/10.4236/fns.2015.615148

Gowen AA, Abu-Ghannam N, Frias J, Oliveira J (2008). Modeling dehydratation and rehydratation of cooked soybeans subjected to combined microwave-hot-air drying. Innovative Food Science and Emerging Technologies 9:129-137.

Justin B, Rani PR, Jitendra P, Stefan C (2015). Drying Characteristics and Moisture Diffusivity of Distillers' Spent Grains Dried in Superheated Steam. Drying Technology 33:15-16.

Kalika G, Alam MS (2014) Mass and cool kinetics of foamed and non foamed grape concentrate during convective drying processes : A comparative study. Journal of Engineering and Technology Research 6(4):48-67.

Katekawa M, Silva M (2006). A review of drying models including shrinkage effects. Drying Technology 24(1):5-20.

Kieu HL, Neli H, Abdolreza K, Andreas B, Evangelos T (2018). Superheated steam drying of single wood particles: A characteristic drying curve model deduced from continuum model simulations and assessed by experiments, Drying Technology 36(15):1866-1881.

Monsurat B, Matthew OO, Victor NE (2019). Modeling of the adsorption isotherm of *Pleurotus ostreatus* using Guggenheim-Anderson-de Boer (GAB) equation. Journal of Engineering and Technology Research 11(4):41-46.

NFX15-119 (1999). Mesure de l'humidité de l'air-Générateurs d'air humide à solutions salines pour l'étalonnage des hygromètres. Association Française de Normalisation (AFNOR).

Pinto LAA, Tobinaga S (2006). Diffusive model with shrinkage in the thin-layer drying of fish muscles. Drying Technology 24:509-516.

Ramirez-Martinez A, Salgado-Cervantes M, Rodriguez-Jimenes G, Garcia-Alvarado M, Cherblanc F, Bénet JC (2013). Water transport in parchment and endosperm of coffee bean. Journal of Food Engineering 114:375-383.

Salmwendé ET, Alfa OD, Guy CT, Kayaba H, Fabien C (2015). Couplage des mécanismes de déshydratation et du retrait de la Spiruline platensis« Arthrospiraplatensis » lors d'un séchage isotherme. Journal de la Société Ouest-Africaine de Chimie 040:17-23.

Seyied MMT, Siroos H, Hamid RT (2015). Effects of Drying Schedules on Physical and Mechanical Properties in Paulownia Wood. Drying Technology 33:15-16.

Tiendrebeogo ES, Tubreoumya GC, Dissa AO, Compaoré A, Koulidiati J, Cherblanc F, Bénet JC, Youm I (2019). Hydric Properties Evolution of Spirulina platensis during Drying: Experimental Analysis and Modeling. Food and Nutrition Sciences 10:516-577.

Vol. 12(1), pp. 24-36, July-December 2020
DOI: 10.5897/JETR2020.0686
Article Number: 40108A965063
ISSN: 2006-9790

http://www.academicjournals.org/JETR

ACADEMIC JOURNALS
expand your knowledge

Journal of Engineering and Technology Research

Full Length Research Paper

Effect of variation of different additives on some selected properties of silica sand mould for aluminium castings

Sani A. Salihu[1*], Abdullahi Usman[1] and I. Y. Suleiman[2]

[1]Department of Mechanical Engineering, Faculty of Engineering, Kebbi State University of Science and Technology, Aliero, Kebbi State, Nigeria.
[2]Department of Metallurgical and Materials Engineering, Faculty of Engineering, University of Nigeria, Nsukka, Enugu State, Nigeria.

Received 20 January, 2020; Accepted 3 July, 2020

The quality of castings in a green sand mould is influenced significantly by its properties, such as green compressive strength, shear strength, shatter index, compatibility, moisture content, permeability and others which depend on input parameters. Usually, the aforementioned properties of a particular casting differ due to variation in composition of the moulding sand mixtures, sand grain shape and size, bonding capacity of the binder, type and quantity of additives used, etc. The present work focuses on the effect of various additives namely, marula shell powder (MSP), silica flour (SF), corn flour (CF) and shea butter (*Vitellaria paradoxa*) shell powder (SBSP) at different proportions. The quantity of the aforementioned additives for experimentation was varied from 1.0 to 6.0 wt.%. The specimens were tested for moisture contents, green compressive strength, permeability number, shatter index, green shear strength and compatibility. From the obtained test results, all the experimental additives were found to improve the selected moulding properties of the Dukku silica sand. However, moulding sand sample with shea butter shell power 6.0 wt.% (SBSP) and silica flour 3.0 wt.% revealed a better compaction as compared to corn flour and MSP. The presence of silica flour and SBSP in the moulding sand was found to improve sand strength and permeability. Green compression strength, shatter index, and shear strength were found to be highest for the SBSP and SF.

Key words: Moulding sand properties, additives, silica flour, corn flour, marula shell powder, shea butter shell powder.

INTRODUCTION

Casting is a process of pouring molten metal into a mould cavity, which corresponds to the required profile of the part to be produced. The liquid metal cools and solidifies in the mould cavity and is removed for cleaning (AFS, 1963; Beeley, 2001). There are many casting processes, but the most widely used system in the foundry industry is green sand moulding process due to mechanization in many green sand foundries, and is less expensive, but

*Corresponding author. E-mail: sani.aliero@gmail.mail.com.

least accurate when compared with other casting processing like investment casting, shell moulding, vacuum moulding, expanded polystyrene process, centrifugal moulding, and permanent mould casting process (Davies, 1950; Dietert, 1950). The principal constituents of moulding sands are the silica sand grains, binder (clay), moisture, and additives. Green sand consists of high-quality silica sand of 85 to 91% with about 6 to 10% bentonite clay, 2 to 8% water or moisture content and other additives in proper proportion by weight with perfect mixing and mulling in suitable equipment (Anon, 1962; AFS, 1963; Yakinni et al., 2015; Jain, 2003) and for defects free cast products, foundry sand for mould making must be carefully prepared to meet certain basic requirements such as permeability, green strength, dry strength, refractoriness, cohesiveness, thermal stability and reusability.

Additives play a very important role for enhancing specific mould properties of the green sand mould like permeability, dry shear strength, green shear strength, green compression strength, and dry compression strength. Ananthapadmanabham et al. (2017) and Chavan and Nanjundaswamy (2013) investigated the sand moulding properties of olivine sand affected by addition of different additives like fly ash, coconut shell ash, and tamarind powder. They observed that, the mould permeability was highest with fly ash, while compression strength was maximum with coconut shell ash when compared with fly ash and tamarind. Sobczak and Purgert (2002) worked on the use of fly ash an aggregate for foundry sand mould and core production. They concluded that fly ash can be utilized as a replacement and filler in foundry sands used in both green and dry sand moulds and also for core production. The moulds made from such foundry sands were successfully poured in many metals in include Fe-, Cu-, Al- and Zn based alloys. For green sand moulds, all investigated fly ashes were found capable of being added up to amounts of 20% with their technological properties remaining at sufficient levels. This provides an opportunity for obtaining castings of satisfactory quality from sand cast grey iron, silicon bronze, aluminium alloys and zinc alloys.

Ochulor et al. (2017) and Danavath (2018) investigated the effect of aluminium dross and rice husk ash on thermal and moulding properties of silica sand obtained from aluminium rolling mills, Ota and by-product of rice milling obtained from Ifo. They concluded that aluminium dross and rice husk ash, both lowered the moulding properties of silica sand when used as an additive. Seidu and Kutelu (2014), Nuhu (2008) and Mehdi (2004) investigated the effect of sawdust, coal dust, and iron fillings on the properties of sand mould. It was found that sawdust with sand mould had higher green strength, but the coal dust containing sand mould exhibited improved sand porosity and permeability and reducing the defects in casting. Moulding sand samples with sawdust additives revealed better compaction; hence improved mould strength requirement is achievable in moulds with sawdust additives. Gadag et al. (1980) investigated the effect of organic additives on the properties of green sand assessed from design experiments and it was found to have higher green strength.

Sand additives are widely used within foundry industry to develop some special property in the sand. From the literature survey, it has been found that the properties of sand mould could be enhanced by addition of few additives (Ayoola et al., 2013; Mahesh et al., 2017). Adachaba et al. (2016) investigated the addition of shea butter to Okenya sand and observed an increased on green compression strength, dry shear strength, shatter index and compatibility of the sand. Shuaib-Babata and Ariyo (2014) worked on corn flour and molasses individually and result of the investigation revealed a positive influence over shatter index

Meanwhile, cereal binder such as corn flour had been used in foundries to improve green strength of moulding sand through the formation of gelatinous bond. Other benefits obtainable when cereal binders are added to moulding mixtures are improvement in the charring capacity and collapsibility of the mixtures after their exposures to the heat of casting (Olakanmi et al., 2010; Olakanmi and Khan, 2002). Shea butter shell powder (SBSP) and marula shell powder (MSP), which are abundant in Nigeria, are expected to provide the necessary improvement in the functional properties of moulding mixtures. It is therefore considered pertinent to explore their functional properties in order to be able to characterise their viability for further industrial and laboratory applications. It is expected that the positive outcome of the study will be economically beneficial to the foundry sub-sector in Nigeria and other nations.

The results of the effect of additives, such as Silica flour and corn flour on the synthetic mould sand properties of the clay/silica sand, reported in previous studies by Olakanmi et al. (2010) and Shuaib-Babata and Ariyo (2014) were impressive. Therefore, this work is using silica flour and corn flour to compare them with new additives that had very little information in the literature. In addition, this is an attempt to develop new additives that are biodegradable and environmentally friendly and substitute for imported additives to the foundry sub-sector in Nigeria. The scientific contributions of this paper are:

(1) Development of new additives that is biodegradable and environmentally friendly.
(2) Comparative analysis of traditional additives with new additives that is biodegradable and environmentally friendly.

MATERIALS

The materials used for this work is silica sands obtained from Dukku, along river side. The additives used are shea butter

Figure 1. Marula shell powder (Salihu and Suleiman, 2018), corn flour (Wikipedia), shea butter powder, and silica flour (Wikipedia).

Table 1. The chemical compositions of Dukku silica sand samples.

SiO_2	Al_2O_3	NaO	Fe_2O_3	MgO	CaO	K_2O	Na_2O
87.36	0.42	0.89	0.94	0.43	0.57	0.15	0.17

Table 2. Physical-chemical properties of additives used for the work.

Property	Shea butter	Marula	Silica flour	Corn flour
Colour	Milky cream	Light yellow	Milky	Yellowish
Odour	Milky	Nutty aroma	Odourless	Odourless
Boiling point (°C)	-	-	2230	-
Melting point (°C)	-	-	161-1720	-
Bulk density (kg/m^3)	-	-	1490	-
Specific gravity	0.88	0.91-0.92	1.59 - 2.66	-
Viscosity (NSm^{-2})	0.2	-	-	-
Saponification value	-	188-199	-	-
Calorific value	9.00	-	-	-
Iodine value	-	70-76	-	-
Refractive Index	-	1.455- 1.465	-	-
Moisture (%)	0.32	-	-	12.9

(*Vitellaria paradoxa*) shell powder, marula (*Sclerocarya birrea*) shell powder, silica flour, and corn flour and were sourced locally in Kebbi State. Figure 1 shows the additives used for this research. Equipment used were sourced from two places: Nigerian Metallurgical Research Centre, Jos and Federal Polytechnic, B/Kebbi and this include sand mixer, speedy moisture tester, standard permeability tester, standard sand rammer, compatibility tester, universal strength testing machine, weighing balance, shatter index machine, shaker, sieve shaker and sieve stack, measuring cylinder, moulding boxes, rammer, vent wire, permeability meter, crucible furnace, hack saw machine, and wire brush were used.

METHODS

Sand preparation

The silica sands were collected from Dukku, along River Niger tail, washed to remove clay and dirt. The processed silica sands were separately dried and sieved using shaker of different meshes and aperture. The obtained sands were studied with ED X-ray fluorescence analyzer for mineralogical compositions shown in Table 1. Table 2 shows the chemo-physical properties of additives used in this work.

Samples preparations

The chemo-physical properties of shea butter shell powder (SBSP), silica flour (SF), corn flour (CF), and marula shell powder (MSP) were determined. These powders and flours were used as binders on Dukku sand. The chemo-physical properties were determined to know their effects on casting. The chemical composition, sieve analysis, and clay content of Dukku sand were also determined. Twenty four (24) samples were prepared for the laboratory tests from various moulding sand mixture that gives the acceptable moisture content. The sand test samples were prepared in accordance with the standard specification for the preparation of moulding sand test samples using Ridsdale standard sand rammer conforming to imperial (2 diameter × 2 height) or DIN (5 cm diameter × 5 cm height) (Loto, 1990).

Each of the test samples from the mixtures were subjected to the relevant sand mould test parameters such as moisture content,

Table 3. Constituents of Dukku moulding sand additives.

S/N	Additives	Proportion of mould additives (%)	Clay (%)	Water (%)	Moulding sand (%)
1	Marula shell powder	0	12	5	83
		1	12	5	82
		2	12	5	81
		3	12	5	80
		4	12	5	79
		5	12	5	78
		6	12	5	77
2	Shea butter shell powder	0	12	5	83
		1	12	5	82
		2	12	5	81
		3	12	5	80
		4	12	5	79
		5	12	5	78
		6	12	5	77
3	Silica flour	0	12	5	83
		1	12	5	82
		2	12	5	81
		3	12	5	80
		4	12	5	79
		5	12	5	78
		6	12	5	77
4	Corn flour	0	12	5	83
		1	12	5	82
		2	12	5	81
		3	12	5	80
		4	12	5	79
		5	12	5	78
		6	12	5	77

green compression, shatter index, shear strength, compatibility, and permeability. All the tests were performed with use of sand testing equipment at Federal Polytechnic, B/Kebbi, Kebbi State and Nigerian Metallurgical Research Centre, Jos. Silica sands, bentonite, water and additives at different proportions were added to the moulds materials, manually mixed and rammed together, blows were used for each of the ramming operation, and ramming were carried out with sand rammer in accordance with AFS specifications. After removing the samples from the sand rammer, they were tested for moisture content, permeability, green shear strength, collapsibility, Shatter index, and green compressive strength. The results of the additive constituents of the produced moulding sands samples used for the tests are shown in Table 3, while Table 4 is the experimental table for Dukku sand with SBSP, SF, CF, and MSP.

Particle size analysis and determination of grain fineness number (GFN)

The Dukku sand that was collected from different locations was uniformly mixed and washed in water to remove clay and undesirable materials. It was then dried and grain size distribution of the sand was determined with the sieve analyzer. Dried 100 g of the sand was weighed with a weighing balance (Olakanmi et al, 2010). A set of standard testing sieve was used to screen the sand as shown in Figure 2. The sand sample was placed on top of a series of sieves of 1400, 1000, 710, 500, 355, 250, 180, 125, 90, and 63 µm and mesh was shaken for 15 min by electrical vibrator set at 3 Hz. After the shaken period, the grains retained on each sieve and the bottom pan was removed, weighed and their percentages determined. Tables 5 and 6 show the sieve analysis of Dukku sand and local additives, respectively. The AFS grain fineness number was determined by taking the percentage of sand retained on each screen and multiplying each by a multiplier to arrive at the product. The total sum of the product added and divided by the total sum of the percentage of the sand retained on the sieves gives the AFS grain fineness number.

$$\text{AFS grain fineness number} = \frac{Sum\ of\ products}{Sum\ of\ (\%\ weights\ of\ sand\ retained} \quad (1)$$

Grain size and its distribution is determine by shaking a known

Table 4. Experimental Table for Dukku sand with SBSP, SF, CF and MSP.

Mould mixture	A	B	C	D	E	F
Sand (%)	82	81	80	79	78	77
Water (%)	5	5	5	5	5	6
Clay	12	12	12	12	12	6
SBSP (%)	1	2	3	4	5	6
CF (%)	1	2	3	4	5	6
SF (%)	1	2	3	4	5	6
MSP (%)	1	2	3	4	5	6

Figure 2. Georgfischer sieve rack (Ridsdale, 2009).

Table 5. Sieve analysis of Dukku sand.

S/N	Sieve aperture	BSS No	Weight retained	% Weight retained	Product (% weight Ret. × BSS No.)
1	1.400	10	-	-	-
2	1.000	16	2. 97	3.03	48.64
3	0.710	22	11. 11	11. 35	249.92
4	0.500	30	19. 55	19.98	600.00
5	0.355	44	24.55	25.09	1060.84
6	0. 250	60	22.95	23.46	1408.20
7	0. 180	100	7. 03	7. 18	719. 00
8	0.125	150	4.52	4.62	693. 00
9	0.090	200	2.67	2. 72	546. 00
10	0. 063	300	1.17	1.19	360. 00
11	-0. 063	350	1. 30	1. 32	465. 50
Total	-	-	97.82	99.94	6151.10

amount of clean, dry sand downward through a set of 11 standard sieves for 15 min (Loto, 1990). The amount of sand remaining in each sieve is weighed and weights are used to compute and AFS grain fineness index (Chavan and Nanjundaswamy, 2013; Olakanmi et al., 2010).

AFS Grain Fineness Number of the sand $= \frac{6151.10}{99.94}$ = 61.52

AFS = 61.52 ≈ 62

Average grain size = 220 + 210/2 = 215 µm

Clay content of Dukku Sand: 12. 00%

Moulding of sand tests

Moulding sand tests are important that determine different moulding sand properties that affect the final quality of casting. These are the important moulding tests, one is the moisture content test another one is the clay content test, grain fineness test, permeability test, compatibility test, green compression strength test, green shear strength test, dry compression strength test, and hardness test

Table 6. Sieve analysis of local additives.

S/N	Sieve size	Mass retained			
		SBSP	SF	CF	MSP
1	2.00 mm	1. 0	-	-	-
2	1.70 mm	1. 1	-	-	-
3	1.00 mm	3. 3	-	0.9	-
4	710 µm	6. 0	6.1	6.2	6. 0
5	355 µm	61. 0	50.8	56.0	50. 0
6	250 µm	43. 7	45.0	42. 0	40. 0
7	150 µm	20. 0	35.8	25. 0	30.6
8	106 µm	12. 0	12.5	15. 0	13. 0
9	75 µm	10. 0	1. 2	3. 0	1. 0
10	53 µm	20. 8	-	-	-
	Last pan	22.15	-	-	-

Figure 3. Speedy moisture tester.

(Indian Standard of Physical Tests for Foundry Sand, 1997).

Moisture content determination

This property was determined by the speedy Ridsdale moisture content teller. To determine the moisture content, the moisture was set up to warm for 3 min by setting the time switch to 3 min while warming the machine, 50 g of green sands and additives were weighed and spread over the pan of the moisture teller. After 3 min, the machine stopped itself and the pan together with the sand sample was then inserted into the lower part of the machine that holds it in position as fast as possible. The heating time was set for 2 min. The moisture in the moulding sand is thus evaporated. Figure 3 shows the speedy moisture tester used for testing the moisture contents of Dukku sand. After 2 min the machines automatically stopped and pan with dried sand was taken out and put in a cooling place. It was then allowed to cool to room temperature. The cooled sand weighed and moisture content determined as follows:

Taking the initial readings to be L (g)
The final readings at room temperature to be M (g)

Then the percentage moisture content, $= \frac{L-M}{L} \times 100$ (2)

The same procedure was repeated for test samples with varying percentages of silica flour, corn flour, shea butter shell powder, and marula shell powder.

Shatter index

A shatter Index tester was adopted for this test. The standard specimen of size 50 mm diameter and 50 mm height was prepared and kept in the steel tube as in the case of permeability. Moulding sands and additives specimen was rammed in a sample tube and the weight of the sample (150 g) was recorded. The specimen was ejected from the specimen tube by placing it on the shatter index tester and the plunger was used to eject the sand by making a free fall a height of 1.83 m onto the anvil squarely in the centre. The anvil cap was then removed carefully and the sieve assembly lifted off to allow removal of sieve from pan. The sand in the receiver is weighed and the weight of sand remaining on the sieve is taken. The same procedure was repeated for test samples with varying percentages of silica flour, corn flour, shea butter shell powder, and marula shell powder. Figure 4 shows the shatter index machine used for the determination of shatter index values for Dukku sand mixtures. The shatter index was calculated as the percentage of the difference of these two weights. The mass of the sand in the receiver was determined and the shatter index was determined for each mix as follows:

Initial mass, M_1

Mass of sand in the receiver, M_2

Shatter index, $x = \frac{M1-M2}{M1} \times 100$ (3)

The significance of shatter index value was used to determine the toughness and collapsibility of the moulding sand (Loto and Akeju, 1990).

For toughness determination:

Figure 4. Shatter index machine.

Figure 5. Sand test samples for permeability test.

Figure 6. Standard permeability tester.

Shatter index = $W_1/W \times 100$ (4)

For collapsibility:

Figure 7. Sand rammer.

Shatter index = W_1/W; (5)

where W is the weight of specimen and W_1 is weight of sand remaining on the sieve.

Permeability

The quantity of air that passed through a standard specimen of the sand at a particular pressure condition is called the permeability of the sand. It is a physical property of the moulded mass of sand mixture which allows gas to pass through it. It depends upon grain size, grain shape, grain distribution, binder and its content. The apparatus used for the determination of permeability are: electric permeability meter was used to determine this property; stop-watch; standard sand rammer. AFS standard specimen of 50 mm diameter and 50 mm in height were prepared by ramming the required quantity of sand (150) each in a smooth surface tube with three blows of standard rammer. These samples were placed in the mercury cup of the permeability meter in an inverted form. Standard air pressure of 9.8×10^2 N/m^2 and 2000 ml of air were passed through the specimen tube containing the specimen. The machine was put on and the pressure lever was pushed, the readings were recorded when the arrow indicator was stable and represent the permeability number. The same procedure was repeated for test samples with varying percentages of silica flour, corn flour, shea butter shell powder, and marula shell powder. Figure 5 shows the test samples for permeability test while Figures 6 and 7 show standard permeability meter and sand rammer for making test samples of 50 mm × 50 mm, respectively.

The permeability number was calculated using the formula:

$$\text{Permeability number (N)} = \frac{V.H}{A.P.T} \quad (6)$$

where V = volume of air that passed through the specimen = 2000 cm^3, H = height of the test specimen = 5 cm, A = cross-sectional area of the test specimen = 19.63 cm^2, P = air pressure in cm of water = 9.8 cm, and T =time taken by the air to pass through the sand specimen (s).

Green compressive strength

This is the property of moulding sand which concerns the strength of the mould while in moist condition at deformation. The strength depends on the degree of ramming, the moisture of the sand and the granulation composition of the sand. The specimens were

Figure 8. Sand samples for green compression test.

Figure 9. Sand rammer for making sand test sample.

Figure 10. Universal sand strength testing machine.

prepared using standard sand rammer and specimen tube

Figure 11. Samples of test specimens.

accessories. The sizes of the specimens were 50 mm × 50 mm. The specimens were placed in between two self-aligning compression heads on the universal testing machine. A uniformly increasing load was applied, while the magnetic rider moved along the measuring scale. As soon as the sample reaches its maximum strength, the sample fails. The magnetic rider remained in position of the ultimate strength while the load was gradually released; the green compression strength for the sample was recorded from the position of the magnet. The same procedure was repeated for samples with varying % of silica flour, corn flour, shea butter shell powder, and marula shell powder. Figure 8 shows sand samples for the test, while Figures 9 and 10 respectively show pictures of sand rammer and universal strength testing machine used the determination of green compression strength of Dukku sand. Green compression strength is calculated as follows:

$$\text{Green compression strength, gf/mm}^2 = F/A \quad (7)$$

where F = load at rupture in gf and A = cross-sectional area of the test specimen in mm^2.

Green shear strength

Green shear strength indicates the strength of the mould during the removal of pattern. The universal testing machine as shown in Figure 11 was fitted with a different adapter in order that loading can be made for the shearing of the rammed sand specimens. Specimen pads used for measuring the shear strength are different from the specimen pads used for measuring the compressive strength because of the replacement of compression head with shear head in the machine. The green shear strength was recorded at the point of failure of the sample loaded. The stresses required to shear the specimens along the axis were determined and recorded as the green shear stress.

Compatibility

The compatibility indicates the water tempering degree of the green sand moulding. Compatibility is the percentage decrease in height of a loose mass of sand under the influence of a controlled compaction. Compatibility test was carried out to know the way moulding sand will withstand repeated cycles of heating and cooling during casting operations. How compatibility test is carried out.

An empty sand sleeve with the stopper plugged underneath it is placed under the funnel outlet of the compatibility tester's sieve as shown in Figure 12. The sand is sieved until a heap is formed. The heap is then stickled off the sand. The sand is rammed four times and the value X is read off the calibration. The compatibility value is then calculated as:

$$\text{Compatibility} = X.100/67. \quad (8)$$

Figure 12. Compatibility tester

RESULTS AND DISCUSSION

The influences of additives addition on Dukku moulding sand properties for all the mixes are as shown in Figures 13 to 18. This display the variation of green compressive strength, moisture content, permeability, green shear strength, shatter index, and compatibility wt.% silica flour, corn flour, marula shell powder (MSP), and shea butter (*V. paradoxa*) shell powder (SBSP). Figure 1 shows the variations of different additives verses green compression strength obtained from Dukku sand mould. As observed, with increase of silica flour additive the green compression strength also increase from wt. 1 to 6%. This might have shown adequate moisture contents with increasing additives that caused the strengthening of compressive strength. Also, there were similar trends observed with marula shell powder (MSP), corn flour, and shea butter shell powder (SBSP). However, in comparing the four additives, shea butter shell powder with 178 kN/m^2 and silica flour with 180 kN/m^2 have shown better compression strength at 6% additive percentage as compared to corn flour and MSP with 170 and 167 kN/m^2, respectively. This might be due to better mould compaction as a result better moisture absorbing strength of SBSP and silica flour. These properties exhibited by both samples are in agreement with the America Foundrymen Standard (AFS, 1963).

Figure 14 shows the variations of these four individual additives on the permeability of the moulding sand. Permeability values could be seen to be increasing as the SBSP, MSP, CF, and SF contents increased, as shown in Figure 14. With increase of percentage of additives the permeability number of SBSP increases from 135 to 155 while silica flour additive increases from 141 to 156. This could be attributed to the replacement of the pore spaces in the sand by the corn flour, and MSP thereby reducing its permeability. Generally, the variations in permeability of the moulding sand as observed are direct consequence of the specimens' constituents. An increase in permeability indicates a more open structure and can lead to rough casting surface, burn-in and metal penetration, while a decrease in permeability is an indication of too tight a packing indicating moulds are prone to blow holes, pin holes, and gas roughened surface.

Figure 15 shows the effect of different additives versus moisture content obtained from Dukku sand mould. The moisture content of silica flour (SF), MSP corn flour (CF) and SBSP increases from 3.5 to 3.98%, 3.5 to 3.88%, 3.5 to 3.85 and 3.5.0 to 4.0%, respectively. It shows that with increase of percentage additives, the moisture content increases. This increase could be attributed to decrease in plasticity of the specimen hence the need for more water to create necessary bonding between the moulding specimens. As observed, 3% SBSP additive reveals the highest moisture content of 4%. But the moisture content of corn flour reduced from 3.5 to 3.2, MSP from 3 to 5 to 3.3, SBSP and SF both reduced from 3.5 to 3.4 with addition of 6% added as additives, respectively as in increased in plasticity with the addition of these additives. This trend was also noticed by the investigations as indicated by Aribo (2011).

The results of the green shear strength of the sand mixes prepared in varying proportion of SBSP, MSP CF, and SF contents is presented in Figure 16. It shows that the shear strength increases as SBSP, MSP, CF, and SF contents increase from 70, 82, 90, 88, 90, 98 and 99 kN/cm^2 for the SBSP. As observed, with increase of percentage additives, the green shear strength values increased in a uniform manner. The relative improved of shear strength of the moulding sand specimens may have been influenced by the effects of constituents of the additives as observed by Sahoo et al. (2017), Olakanmi et al. (2010) and Aribo (2011). As observed from Figure 16 that the green shear strength attained its maximum values when 6% of SBSP and MSP additives were used on the moulding sand as compared to other additive (silica) because of finer size and better moisture absorption capacity.

Figure 17 shows the variation of different additives versus percentage compatibility. The effects of weight % additives moulding sand specimen on compatibility shows that with increase of percentage additives the compatibility also varies. There was shape increase from 0 to 1%, and 2%, then followed by decrease from 3, 4, 5 and 6% with MSP and corn flour attaining the lowest 30% compatibility, while silica flour had 45% compatibility. It shows that the SBSP, MSP, CF, and SF reveal that the optimum compatibility occurs at 1 and 2%.

Figure 18 shows the variation of wt.% additives content versus the shatter index. The shatter index is critical to the strength requirement of the sand moulds. As observed from Figure 18, with increase of wt.% additives the shatter index increased. The shatter index of SBSP increased from 50 to 80.0% while the MSP index creased from 50 to 73% on addition of 1 to 6 wt.%, respectively. The corn flour additive and silica flour had the least shatter index of 62%. SBSP sample shows a value of

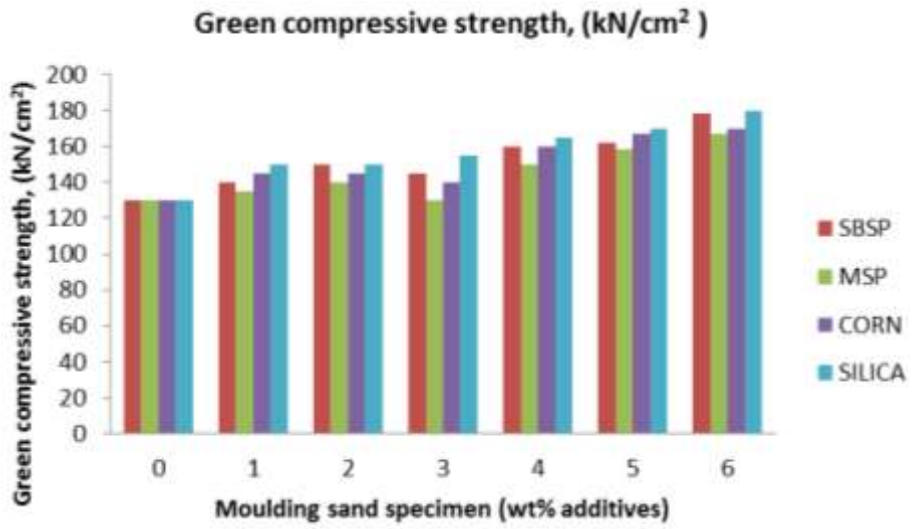

Figure 13. Variation of green compressive strength at different percentages of additives.

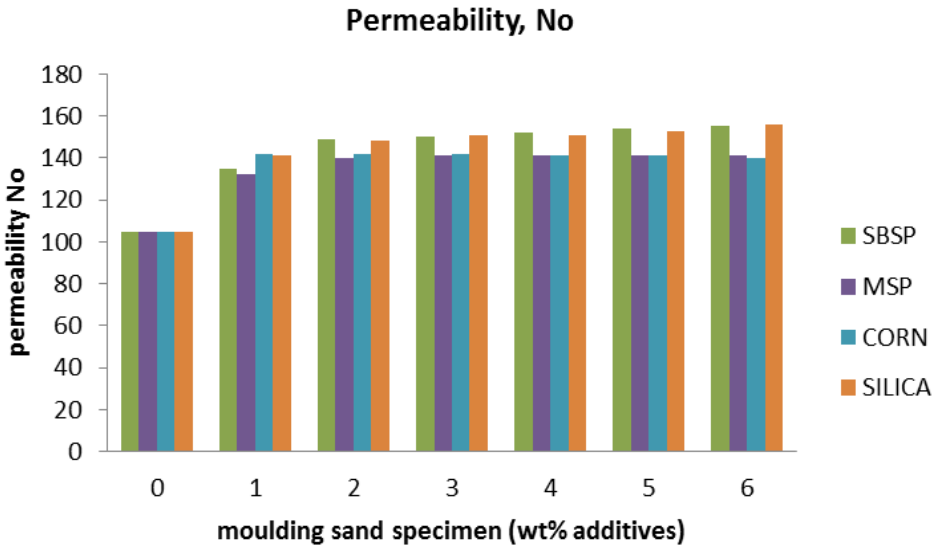

Figure 14. Variation of permeability number with different percentages of additives.

80%.

Effect of additives

The effect of additives is apparent from all the results obtained as presented in Figures 13 to 18. The additives increased the green compressive strength, permeability, moisture content, shear strength, compatibility, and shatter index of the Dukku moulding sand and hence improve on the properties and quality of casting. The individual effect of the additives is as shown in Figures 13 to 18.

Conclusions

Based on the results of the moulding sand properties from Dukku River in this study, the following conclusions are made:

(1) All the experimental additives were found to improve the selected moulding properties of the Dukku silica sands, that is, green compressive strength, moisture content, permeability, compatibility, shatter index, green shear strength, and porosity, and therefore can be incorporated as moulding sand additive depending on the structure desired in the final cast product.

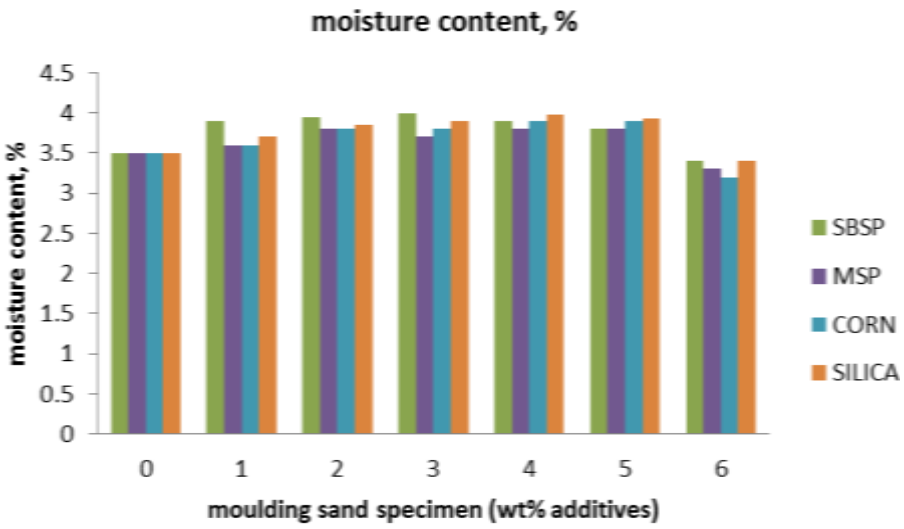

Figure 15. Variation of moisture content at different percentages of additives.

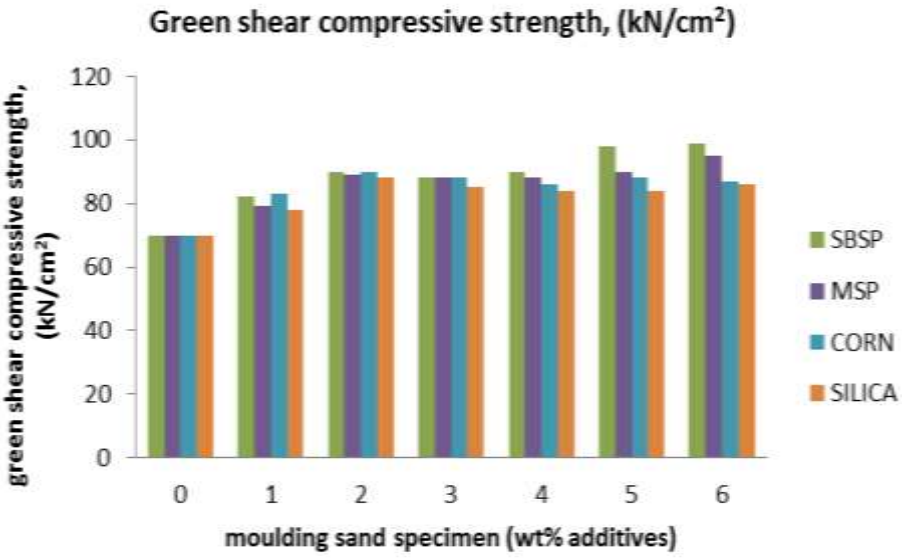

Figure 16. Variation of green shear strength at different percentages of additives.

(2) Moulding sand specimens from Dukku with silica flour and SBSP additives revealed a relatively better compaction. Hence, improved mould strength is achievable in moulds with silica flour and SBSP additives.
(3) The presence of silica flour and SBSP in the moulding sand was found to improve sand permeability. Therefore, relative less casting defects including blow hole may be obtained with moulding sand that is rich in silica flour and SBSP.
(4) The presence of SBSP and SF in the moulding sand was also found to improve the green compressive strength better than the corn flour and marula shell powder. However, SBSP and MSP were found to have better shatter index than the silica flour and corn flour.

CONFLICT OF INTERESTS

The authors have not declared any conflict of interests.

ACKNOWLEDGEMENTS

The authors express their thanks to the TetFund for the

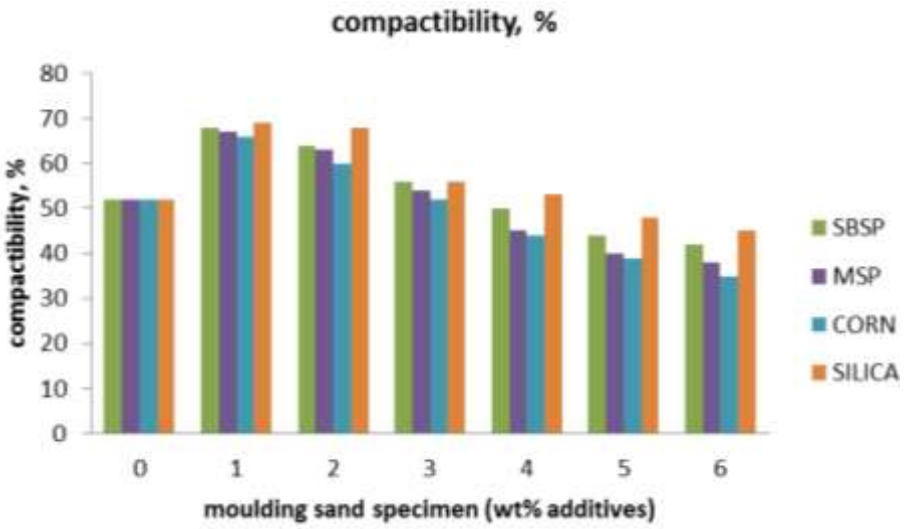

Figure 17. Variation of percentage compatibility with different % of additives

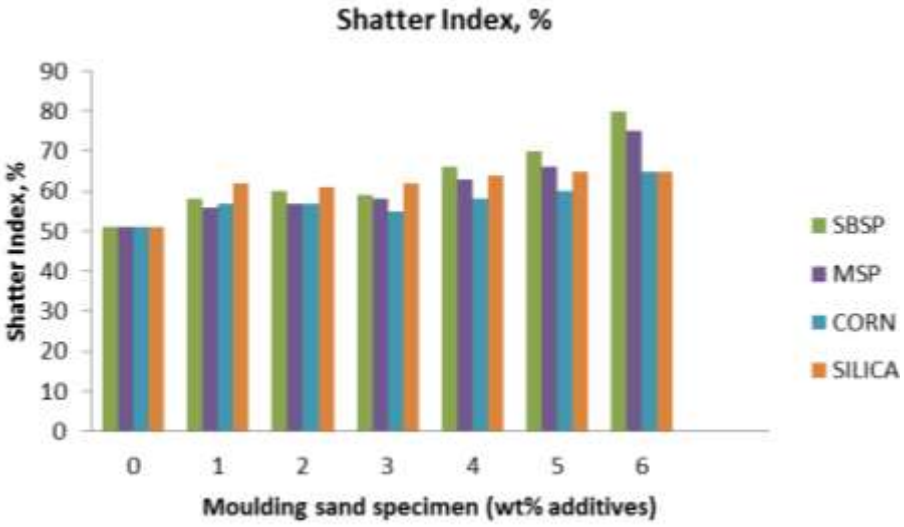

Figure 18. Variation of shatter index versus different percentages of additives.

financial support, Kebbi State University of Science and Technology, Aliero (KSUSTA), Federal Polytechnic, B/Kebbi, Staff of Mechanical Engineering Department, Kebbi State University of Science and Technology, Aliero, for the support and encouragement during research studies, and National Metallurgical Development Centre (NMDC), Jos.

REFERENCES

Adachaba A, Oloche OB, Tuleun LT, Gundu DT (2016). Shea butter (Vitellaria paradoxa) binder addition to Okenya sand in Kogi State, Nigeria and its effects on moulding properties of the sand. Journal of Multidisciplinary Engineering Science and Technology 3:1.

American Foundrymen's Society Inc. (AFS) (1963). Mould and core test handbook, 7th edition, New York.

Ananthapadmanabham KC, Dharshan BG, Somashekar R (2017). Effect of additives on silica sand mould for aluminium castings, International conf. on Current Trends in Engineering, Science, and Technology, ICCTEST, GRENZE Scientific Society.

Anon (1962). Moulding materials and methods. 1st edition, AFS, Chicago, USA.

Aribo S (2011). "Effect of varying corn cob and rice husk ashes on properties of moulding sand". Journal of Minerals and Materials Characterisation and Engineering 10(15):1449-1455.

Ayoola WA, Adeosun SO, Oyetunji A (2013). Investigation into foundry properties of Oshogbo and Saki silica sand deposits. International journal of engineering. Fascicule 3, Hunedoara, Romania pp. 213-218.

Beeley PR (2001). Foundry technology, 2nd edition, London, Butterworth-Heinemann.

Chavan TK, Nanjundaswamy HM 2013). Effect of variation of different additives on green mould properties for olivine sand. International Journal of Research in Engineering and Advanced Technology 1:4.
Danavath B (2018). Analysis of foundry raw materials. International Research Journal of Engineering and Technology 05(09):146-156.
Davies W (1950). Foundry sand control. Testing Research Department, United Steel Companies, Humphries Limited, London.
Dietert HW (1950). Foundry core practice. Chicago, American Foundrymen's Society. https://www.amazon.com/Foundry-core-practice-Harry-Dietert/dp/B002HLVJ8W
Gadag SP, Rao KS, Srinivasan MN, Seshan S (1980). Effect of organic additives on the properties of green sand assessed from design experiments. Indian Institute of Science, Bangalore, Transactions of the American Foundrymen's Society pp. 177-182.
Indian Standard Methods of Physical Tests for Foundry Sands (1997). Bureau of Indian Standards, Manak Bhavan, 9 Bahadur Shah Zafar Marg, New Delhi.
Jain PL (2003). Principles of foundry technology, 4th edition, New Delhi, Tata McGraw publishing company.
Loto CA (1990). Effect of cassava flour and coal dust addition on the mechanical properties of a synthetic moulding sand. Applied Clay Science 5:249-263.
Loto CA, Akeju EA (1990). Durability of Igbokoda Clay and Silica Sand as a Synthetic Moulding Sand. Applied Clay Science pp. 21-29.
Mahesh G, Sai Krishna K, Naveen Kumar S, Suresh S, Sanjay Kumar S (2017). Analysis and optimization of various mould attributes in sand casting. International Journal of Engineering Technology Science and Research 4(12):1335-1340.
Mehdi D (2004). Mold sand, sand additives and sand properties. IUST. http://meteng.iust.ac.ir/files/mateng/divandari_3a69a/files/0000-Divandari-sand.pdf
Nuhu AA (2008). Evaluation of the foundry properties of river Niger sand behind Ajaokuta steel company limited, Ajaokuta, Nigeria. American-Eurasian Journal of Scientific Research 3(1):75-83.
Ochulor EF, Amuda MOH, Adeosun SO, Balogun SA (2017). Effect of aluminium dross and rice husk ash on thermal and moulding properties of silica sand. Nigerian Journal of Technology 36(3):794-800.
Olakanmi EO, Aiyeru SG, Idalu PI (2010). Effect of cereal binder, moisture, and clay contents on the functional properties of clay-bonded core and moulding sands. South African Journal of Industrial Engineering 21(2):217-230.
Olakanmi EO, Khan RH (2002). Investigation of the moulding and core-making properties of some locally available foundry sands, Journal of Science, Technology, and Mathematics Education 5(2):67-75.
Ridsdale D (2009). Foundry sand testing equipment operating instruction (Metric), https://www.basrid.co.uk/ridsdale/images/pdf/Metric_OIM.pdf
Sahoo K, Pattnaik S, Sutar MK (2017). Effect of different additives on some selected properties of green sand mould. International Journal of Engineering Technology Science and Research 4(9):1430-1433.
Salihu SA, Suleiman IY (2018). Comparative analysis of physical and chemical characteristics of selected clay deposits found in Kebbi state, Nigeria. International Journal of Physical Sciences 13(10):163-173.
Seidu SO, Kutelu BJ (2014). Effect of additives on some selecteted properties of base sand. Journal of Minerals and Materials Characterization and Engineering 2:507-514.
Shuaib-Babata YL, Ariyo DO (2014). Effect of local additives on engineering properties of Okelele-Ilorin (Nigeria) clay. IOSR Journal of Mechanical and Civil Engineering 11(3):37-42.
Sobczak J, Purgert RM (2002). The use of fly ash as an aggregate for foundry sand mould and core production. Energy Industries of Ohio park centre plaza, suite 200. https://silo.tips/queue/the-use-of-fly-ash-as-an-aggregate-for-foundry-sand-mold-and-core-production?&queue_id=-1&v=1598627714&u=MTk3LjIxMC4yMDIuMTYy
Yakinni AA, Bello SK, Animashaun LA, Olaiya KA (2015). Assessment of mechanical properties of foundry moulding sands. International Journal of Engineering Innovation and Research 4(2):365-371.

Vol. 12(1), pp. 37-46, July-December 2020
DOI: 10.5897/JETR2020.0695
Article Number: 84C7C5A65235
ISSN: 2006-9790

http://www.academicjournals.org/JETR

ACADEMIC JOURNALS

Journal of Engineering and Technology Research

Full Length Research Paper

Effective use of Quadcopter drones for safety and security monitoring in a building construction sites: Case study Enugu Metropolis Nigeria

Okaka O. Patrick[1*], Ezekiel O. E. Nnadi[2] and Henry C. Ajaelu[2]

[1]Building Technology Department, School of Environmental Technology, National Institute of Construction Technology and Management (NICTM), Federal Polytechnic Uromi, Edo State, Nigeria.
[2]Department Quantity Surveying, Faculty of Environmental Sciences, Enugu State university of Science and Technology (ESUT), Agbani, Enugu State, Nigeria.

Received 9 May, 2020; Accepted 14 July, 2020

The hazardous nature of the Nigerian building construction industry due to lack of construction data and records of incidents which have led to loss of life, property damage, injuries and loss of materials in an average construction site is alarming. The aim and objective of this study is to know how effective the use of drone to monitor safety and security in Nigerian Building Construction site can improve dangerous site situations. In other to achieve the aim and objective of this study the following were postulated: To examine the level of awareness of drones in Enugu State Nigeria? What is the level of adoption of drones among construction stakeholder in Enugu State Nigeria? To examine the limitations of using drones/UAVs (Quadcopter) for safety and security monitoring within Building Construction sites in Enugu State Nigeria. Genius-idea drones and DJI Phantom 3 Standard Drones were used in this study. The targeted professionals/stakeholder was architects, builders, engineers, quantity surveyors, land surveyors, estate surveyors and clients. However, 242 people responded to the questionnaire. Data collated was analyzed using statistical package for social sciences (SPSS) computer software version 23.0 for windows. However, 66% of respondents were aware of drone concept in construction monitoring while 51% respondents adopted drones in different sectors of construction monitoring. However, in safety and security monitoring 17.6% adoption was indicated as low between stakeholders in the Enugu State Building Construction industry. The use of drones in the developed world namely America, Europe, China, Australia and India have been employed in safety and security monitoring and in construction progress monitoring of both high rising and vast projects with great success. In the Nigerian perspective, drones as a tool for monitoring safety and security of all phases of construction are still at the nascent stage. The effective use of drones in Nigeria is encouraged since reality imagery collected from drones could be used for analyzing and evaluating of ongoing construction activity like planning movement on site and monitoring materials on site and could be stored for future references.

Key words: Quadcopter drone (UAV), reality images, safety and security monitoring, DJI Phantom 3 standard.

INTRODUCTION

The hazardous nature of the Nigerian building construction industry due to lack of construction data and records of incidents which have led to loss of life, property damage, injuries and loss of materials in an average building construction site is alarming. (Grayson, 2015) refers to the aircraft itself or equipment operated

independently of human control. Initial uses for UAVs were primarily for military purposes and military research has been a major driver for advancing UAV technology. Moreover, the advancement of GPS technology has allowed both military and civilian UAVs to be navigated by satellite (Carrison, 2015). Small multi-propeller helicopters called “quadcopters” can be equipped with almost any sensing technology (Snider and Welch, 2015). Drone has improved productivity in agriculture, construction project deliver process, forestry safety and security (Wallace et al., 2014; Andrea et al., 2010). Drone can be used to reach heights that humans can’t reach. While inspecting a leaking roof you can send a drone to take picture and single out the damaged point for further repairs. Drone can be used to inspect high rise buildings without obstruction of work. Unmanned aerial vehicle is capable of capturing numerous photos from various angles and zoom settings in a matter of minutes. The entire operation is conducted without road closures, at greatly lower cost than alternative inspection techniques, and with very little safety risk (Pritchard, 2015). Wind turbine inspections have traditionally been accomplished through the use of binoculars or by technicians that are required to climb to great heights. The introduction of UAVs has provided a much safer option for these inspections and with higher resolution than that offered by binoculars (NAW Staff, 2015). Using drones allows you to have more real-time detailed control over the project, so you can keep track of the progress visually, and achieve closure at perhaps a quicker time than previously estimated (Irina et al., 2018).

According to Ezeokoli et al. (2016), the Nigerian Construction industry is a well-known late comer to the adoption of innovations compared to other sectors. The digital revolution faced by construction industries at this time is a paradigm shift in the use of technologies, aimed at increased productivity, efficiency, value, quality, sustainability and reduced lifecycle costs. The traditional safety monitoring of construction projects lacks a good number of trained staffs and taskforce. However, lots of safety and security incidents have gone undocumented. The indigenous construction professionals and client pay little or no attention to safety and security in an average Nigerian construction site making it risky and accident prone. Government policies and lack of enforcement has made the situation worsen in recent times.

The aim of this study is to know how effective the use of drone to monitor safety and security in Nigerian Building Construction site can improve dangerous site situations and reduce material loss on site. In other to achieve the aim, the following objectives were raised: To examine the level of awareness of drones in Enugu State Nigeria? What is the level of adoption of drones among construction stakeholder in Enugu State Nigeria? To examine the limitations of using drones/UAVs (Quadcopter) for safety and security monitoring at selected building construction site in Enugu Metropolis.

RESEARCH METHODOLOGY

In this study, investigations were carried out on the use of Quadcopter drones (unmanned aerial vehicles) as a tool for monitoring Safety cultures of workers on the building construction sites through reality images and video streams captured by DJI Phantom 3 and genius-Idea drones. The researcher selected these drones because of the high quality of pictures and availability of drones in the research area. However, DJI enterprise makes drones with features that ease data collection in the construction sites. The genuine Idea drone is a recreational drone that was used as backup flight in the survey.

Genius-idea drones and DJI Phantom 3 standard drones with the following specifications were used in this study: Genius-idea drone taking off weight 275 g, maximum used altitude 3000 m, endurance time 20 min, video resolution ratio 4 K;1080 P and 720P, controlled with an android phone or an iPhone with the help of G-idea app. The requirements for the versions in mobile equipment system is android 4.3 and above or iOS 8.0 and above. While the DJI Phantom 3 standard maximum tested altitude is 500 m, endurance time 25 min, it has an integrated 3-axis Gimbal stabilization with photo resolution 12 mp, Shutter speed 8 to 1/8000 s, video resolution FHD (1920 x 1080), high density (1280 x 720), package weight 0.65kg, recording media: micro SD 64GB, operating temperature 32 to 40°F/ 0 to 40°C. It also comes with a remote controller.

Site location

Enugu State is one of the states in south-eastern Nigeria. Its capital is Enugu. The state was created in 1991 from the old Anambra State. Enugu state is located within latitude 06^{o} 00’N and 07^{o} 00’N and longitude 07^{o} 00’E and 07^{o} 45’E. The state is called the Coal City State because of the discovery of coal in a commercial quantity in Enugu Urban in 1909. Enugu was then the capital of Eastern Nigeria. However, the two estates used in this research work for observation purposes are Devine Hectares estates and WTC estate. Devine hectares estate is new and located with this latitude 6°25’39” N_7°31’13” E inside Centenary City, Enugu State Golf and Lifestyle City. Centenary City is Located at Enugu-South KM7, Enugu, Port-Harcourt Expressway. Devine hectares estate comprises of duplexes and few bungalows that are prototype residential buildings. The estate has its own estate manager and engineers. The estate is divided into Phase 1, 2, 3 and 4. Phase 1 and 2 are developed with some built up area and about 160 plots while 3 and 4 have not been developed at the point of this research work. While WTC estate is located in the center of Enugu State close to Uba Bus stop, Ogui, Enugu State Nigeria. The semidetached bungalow located in this latitude 6°25’36N _ 7°30’14” E was observed in this research work.

Batching of flight timing

The flight dispatch was scheduled into two batches morning and

*Corresponding author. E-mail: tiendrebeogoeloi@yahoo.fr. Tel: (+226) 50 30 70 64/65.

Figure 1. Genius-idea drone picture during calibration onsite.
Source: Field survey 2019.

evening to monitor the activities at work during the commencement of work and at the end of work. Work started on site by 8:00 hour and two hours into the work 10:00 hour the first inspection was conducted, and another inspection was conducted to know the last condition and positions of materials on site around 5:00 hour before handing over to the site/estate security.

Questionnaire

Opinion pool were sought and questionnaire was prepared with goggleform (www.googleform.com) for the use of drones for effective monitoring of safety culture in the building construction sites and was distributed to the professionals in the construction industry through SMS, WhatsApp, Facebook messenger and field distribution. The targeted professionals were Architects, Builders, Engineers, Quantity Surveyors, Land Surveyors, Estate Surveyors and clients. However, 242 people responded to the questionnaire. Data collated was analyzed using statistical package for social sciences (SPSS) computer software version 23.0 for windows. Descriptive statistics which includes frequency and percentages were used to summarize categorical variables while means and standard deviations were obtained for continuous variables. The Likert scale was ranked from code 1 = strongly disagree/very difficult/very slow to code 5 = strongly agree/very easy/very fast. Mean greater than the criterion means of 3 was regarded as a positive response and vice-versa.

RESULTS

Figures 1 and 2 show the picture of drones used in this study. The DJI drone was used more onsite because it is easy to control it gives a stable and high-resolution imagery. The genius-idea drone calibration was not successful due to poor GPS signal onsite.

Location

Divine Hectares Estate is a large estate with about 800,000 m^2 for phases one, which is about 160 plots. The property is being developed by geo-square meter (private developers) it runs into phases 1 to 4. Figures 3 and 4 show an aerial view of Divine Hectares Estate.

Batching of flight time

Flight dispatch was scheduled into two batches morning and evening to monitor the activities at work during the commencement of work and at the end of work. Images captured by the UAV during commencement of work showed that five workers in the foundation were not wearing their Personal Protective Equipment's (PPE) while mixing concrete and laying blocks in the foundation. Figure 5 shows the aerial view of the foundation. Figure 6 also shows workers on a duplex without any safety wears as well.

Figures 7 and 8 show activities covered on site. Data collected through drone inspection during site closure around 17:00 hours showed materials and equipment positioning on site before handing over to the site security.

Questionnaire

The response to the various questions from the questinnaire are peresented in Figures 9. Figure 9 shows

Figure 2. DJI drone Phantom 3 Standard captured onsite with an android phone.
Source: Field survey 2019.

Figure 3. Aerial view of devine hectares estate from entrance.
Source: Field survey 2019.

that 66% of the respondents in the building construction industry are aware of UAV concept. Table 1 shows that out of 51 professionals that use UAVs in project monitoring, only 3 (5.9%) use it often while 30 (58.8%) use it occasionally. The kind of projects they use UAV include: Surveying mapping (29.4%), construction project monitoring (23.5%) and safety and security monitoring (17.6%). The respondents that owned drones more were

Figure 4. Aerial view of devine hectares estate.
Source: Field survey 2019.

Figure 5. Worker in the foundation working without their personal protective equipment and the foundation basket dropped carelessly on the floor, captured by a DJI Phantom 3 Standard drone.
Source: Field survey 2019.

land surveyors, an architect and a builder which added up to 17.6%. The type of drones owned by them includes DJI Phantom 4 Pro (33.3%), Geniusidea drone (33.3%) and Phantom 3 standard (33.3%). The table also reveals that 58.8% of the respondents have been trained on how to fly a drone. Most of the training took place online (40%) and in Nigerian Institute of Surveyors training section (20%).

Table 2 shows that the respondents outlined various UAV adoption limitations. They include: Poor performance of drones in extreme weather conditions (3.67), battery life and limited flight time (3.78), communication loss (3.39), laws and regulations with restrictions (3.57), labour and work distractions (3.08), privacy concerns

Figure 6. Workers in the upper floor were not wearing any Personal Protective captured by DJI drone.
Source: Field survey 2019.

Figure 7. Samples of materials on site captured by a DJI Phantom 3 Standard drone during closing of work.
Source: Field survey 2019.

Figure 8. Aerial reality image of material and equipment onsite during closing hour including offcuts scattered on the floor. captured by a DJI Phantom 3 Standard drone.
Source: Field survey 2019.

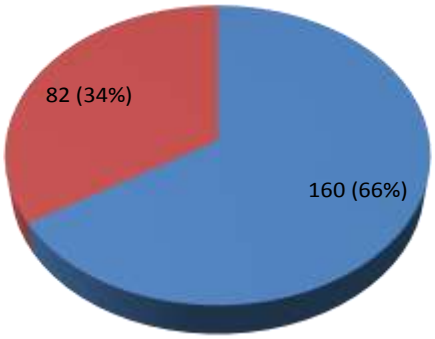

Figure 9. Awareness of UAV concept among stakeholders.
Source: Field survey 2019.

Table 1. Level of adoption of UAVs by stakeholders in building project safety and security monitoring.

	Frequency	Percent
If yes in what frequency		
Occasionally	30	58.8
Often	3	5.9
Rarely	15	29.4
Very often	3	5.9
What kind of project does use UAV for?		
Safety and security monitoring	9	17.6
Construction project monitoring	12	23.5
Event coverage	15	29.4
Surveying/mapping	15	29.4
Do you own a drone?		
Yes	9	17.6
No	42	82.4
If yes specify the type		
DJI Phantom 4 Pro	3	33.3
Geniusidea drone	3	33.3
Phantom 3 standard	3	33.3
What is the cost range of owning a drone?		
1000-2000$	3	33.3
2000-3000$	3	33.3
50-1000$	3	33.3
Have you undergone any training on flying a drone both formal and informal?		
Yes	30	58.8
No	21	41.2
If yes specify where u had the training		
Enugu State	3	10.0
Nigerian Aviation School Zaria	3	10.0
NIS training section	6	20.0
NIS workshop	3	10.0
Online/YouTube	12	40.0
Private training	3	10.0

Source: Data adopted from Field survey 2019.

Table 2. Limitations of adopting effective use of Quadcopter drones in safety and security monitoring in building construction sites.

	Strongly disagree n (%)	Disagree n (%)	Moderate n (%)	Agree n (%)	Strongly agree n (%)	Mean ± SD
Drones do not function well in extreme weather conditions	0 (0.0)	18 (7.4)	83 (34.3)	101 (41.7)	40 (16.5)	3.67 ± 0.84
Battery life and limited flight time	3 (1.2)	6 (2.5)	83 (34.3)	99 (40.9)	51 (21.1)	3.78 ± 0.85
Communication loss	3 (1.2)	27 (11.2)	111 (45.9)	75 (31.0)	26 (10.7)	3.39 ± 0.87
Laws and regulations with restrictions	3 (1.2)	32 (13.2)	67 (27.7)	105 (43.4)	35 (14.5)	3.57 ± 0.94
Accident and property damage	12 (5.0)	59 (24.4)	116 (47.9)	32 (13.2)	23 (9.5)	2.98 ± 0.98
Loss of Life	44 (18.2)	120 (49.6)	59 (24.4)	17 (7.0)	2 (0.8)	2.23 ± 0.86
Labour and work distractions	3 (1.2)	67 (27.7)	98 (40.5)	55 (22.7)	19 (7.9)	3.08 ± 0.93
Privacy concerns	3 (1.2)	37 (15.3)	84 (34.7)	87 (36.0)	31 (12.8)	3.44 ± 0.94
Low quality images	18 (7.4)	97 (40.1)	73 (30.2)	45 (18.6)	9 (3.7)	2.71 ± 0.98
Must be operated by a competent person	3 (1.2)	18 (7.4)	58 (24.0)	56 (23.1)	107 (44.2)	4.02 ± 1.05
Blurring images	6 (2.5)	50 (20.7)	132 (54.5)	51 (21.1)	3 (1.2)	2.98 ± 0.75
Water resistance	0 (0.0)	46 (19.0)	133 (55.0)	60 (24.8)	3 (1.2)	3.08 ± 0.69
Causes distraction in working environment /construction site	9 (3.7)	46 (19.0)	92 (38.0)	69 (28.5)	26 (10.7)	3.24 ± 1.00

*Means greater than criterion mean of 3 indicates Agreement and vice-versa.
Source: Data Adapted from Field survey 2019.

(3.44), must be operated by a competent person (4.02), water resistance (3.08) and causes distraction in working environment/construction site (3.24).

DISCUSSION

This study adopted and agreed with the modalities reported by Naveed et al. (2018) for successful drone operation. The inspection of UAV is necessary before site activities are commenced. Monitoring of the environments or locating hazard free zones for flight should be done on site. Special attention should be paid to safety requirements of the environment (people nearby, surrounding buildings, trees, weather conditions, especially wind and humidity, etc.) and the UAV status (GPS reception, condition of components, status of batteries, motors). From our pilot studies, it is important to make a flight plan based on gathered information obtained at the site visit, to ensure that the pilot and the camera operator become familiar with predefined flight path, camera sequence and locations of image capturing, which are necessary for successful work completion. Take-off point should be on a flat surface to avoid and reduce chances of crash. Before flight, all vital components of the UAV must be checked in order to minimize chances of failures. The pilot can then initiate the flight of the drone to the required inspection point and the camera operator may start capturing high-resolution images via remote control. After the inspection process is finished, the pilot can fly the UAV back fully automatically to the starting point (Rok et al., 2016). Irina et al. (2018) agreed that ensuring compliance with the requirements of the Federal civil aviation administration is required before the use of drone on site. Also, there is need to think about tasks in advance as there are no two identical construction sites so also difficulties encountered, it is important to have a clear idea of what you will do with the information before you collect it, as this will allow you to select the level of detail required to perform the task. Finally, there is need for training of staff or resort to the help of licensed pilots (Naveed et al., 2018). Rok et al. (2016) agreed that traditional monitoring is based on visual examination which is time consuming and technically difficult depending on the size of the site. In large projects it is more expensive to employ safety officers that will monitor workers and provide a platform to secure materials on-site. The process of fuelling the transport system and gathering the workers for inspection might lead to distractions and delay in

project delivery time. McClintock (2019) agrees that drones can execute work with complete accuracy, saving time, effort and money, DJI Phantom 3 standard covered 800,000 m^2 in less than 30 min and provided clearly self-explanatory aerial pictures that can be interpreted by a safety officer and communicated to the site engineers for effective correction during working hours (Figure 3 and 4). Images and video captured by the UAV gives the safety manager valuable documentation of jobsite conditions in cases where accidents do occur, and the UAV provides a tool to cover a larger area of the construction site in a shorter amount of time (Schriener and Doherty, 2015). Figure 5 shows the activities of the number of workers in the foundation, the light circle in the figure indicates that the workers were being monitored and when zoomed it was seen that they were not wearing PPE and also the foundation basket dropped on the working area can cause injury to workers (unsafe act). In Figure 6, workers were captured at an elevated height which is hard to access normally. It also shows that the safety culture in the workplace is below standards thereby putting the workers at risk. Materials and equipment were captured in Figure 7 and 8 at the closing of work as a security picture to mark the state in which the site was, before handing over to the estate security. The disposition of the site implies that materials and machines were in safe conditions. Ingenious (2015) agreed that using a quadcopter drone could enhance security of a construction site. The stream/reality videos used for this research identified movements of workers and their activities during the drone monitoring exercise.

Results from questionnaire shown in Figure 9 shows 66% of respondents were aware of drone concept in construction monitoring. However, Table 1 indicated that 51 respondents adopted drones in different sectors of construction monitoring but safety and security monitoring 17.6% adopting was indicated between stakeholders in the Enugu State Building Construction industry.

The results of this study under these objectives showed that drones do not function well in harsh weather conditions, limited battery life and flight time, communication loss and privacy concern. Mark and Junshan (2017) indicated that there is risk of privacy concern, risk of causing personal injuries and property damage. Rok et al. (2016) also identified that impact on motor vibrations can cause blured images. According to field observation report the DJI phantom 3 standard drone did not crash land nor hit stationed objects, it also did not cause injury to workers because flight path was established considering this limitations metioned. The vibration on the motor did not blurr the images. Drone companies have improved from recreational to commercial drones which carry various types of sensors to suit clients specifications. Drones can be flown in batches like four times to achieve the desired reports thereby complimenting the short flight timing (Naveed et al., 2018). The Nigerian Civil Aviation Authority (NCAA) has put in place Regulations/Advisory Circular to guide the certification and operations of civil RPA in the Nigerian airspace (Nig.CARs 2015 Part 8.8.1.33) and implementing standards (Nig.CARs 2015 Part IS.8.8.1.33); No government agency, organization or an individual will launch an RPA/UAV in the Nigerian airspace for any purpose whatsoever without obtaining requisite approvals/permit from the Nigerian Civil Aviation Authority (NCAA) and Office of National Security Adviser (NSA), in compliance with Irine et al. (2018). Currently in January 2020, legal ristrictions on drones was lifted by the Nigerian Civil Aviation Authority (NCAA), flying a drone is legal in Nigeria provided there is awareness and compliance with the regulations. However, this gives a fair play ground for more drone innovations in the Nigerian Construction Industry.

Conclusion

The effective use of drones in Nigeria is encouraged since data collected from drones could be used for analyzing and evaluating of ongoing construction activity like planning movement on site and monitoring materials on site and could be stored for future references. The use of drones will reduce the rate of building collapse, wastage of materials, inadequate monitoring, and unsafe working environment. Job satisfaction will improve because the client will be carried along in the decision making from any location during the project life-span. Drone/quadcopter as a tool for building construction monitoring, safety and security is adoptable in Nigeria. During the construction activity video streams/pictures showed unsafe conditions on the site and these were communicated to the construction team/workers, and unsafe conditions were averted. The use of Quadcopter is a possible panacea for the effective monitoring of building construction sites. This research proposes use of unmanned aerial vehicles as a viable alternative to the traditional safety and security monitoring in the Nigerian building construction site.

CONFLICT OF INTERESTS

The authors have not declared any conflict of interests.

REFERENCES

Andrea SL, Jeffery EH, Rango A, Winters C (2010). Acquisition, or thorectification, and Object-based Classification of Unmmaned Aerial Vehicle (UAV) Imagery for Rangeland Monitoring. Photogrammetric Engineering and Remote Sensing pp. 661-672.

Carrison T (2015). RC History. 9 1. RCFlightline.com. Retrieved September 1, 2015, from http://www.rcflightline.com.

Ezeokoli FO, Okoye PU, Nkeleme E (2016). Factors Affecting the Adaptability of Building Construction Modelling (BIM) for Construction

Projects in Anambra State. Journal of Scientific Resaerch and Report pp. 1-10

Grayson W (2015). Drones: How Drones and UAVs are Already Affecting Construction Jobsites. http://www.equipmentworld.com/drones.

Irina Z, Smirnova A, Borremans A (2018). “Digital transformation: the case of the application of drones in construction”. MATEC Web of Conferences 193:50-66.

Mark CT, Junshan L (2017). Unmanned Aerial Vehicles in the Construction Industry. 53rd ASC Annual International Conference Proceedings (Copyright 2017 by the Associated Schools of Construction) pp. 383-393.

McClintock O (2019). Guest Post: How Drones Can Be Used For Building Construction. Retrieved from Gettrik.com: https://gettrik.com/guest-post-how-drones-can-be-used-for-building-construction/

NAW Staff (2015). North American Windpower: Report: UAVs for Wind Turbine Inspections to Hit $6 Billon By 2024. Retrieved September 21, 2015, from http://www.nawindpower.com/e107_plugins/content/content.php?content.14613

Naveed A, Izhar MA, Fawad AN (2018). Construction Monitoring and Reporting using Drones and Unmanned Aerial Vehicles (UAVs). The Tenth International Conference on Construction in the 21st Century (CITC-10), 10.

Pritchard L (2015). Pointer Avionics SkyHunter406 - Main. Retrieved from http://www.skyhunter406.com/news.php?action=display&news=48

Rok C, Gic Gradnje DOO, Uros K (2016). "An Unmanned Areal Vehicle for Multi-Purpose Tasks in Construction Industry." Journal of Applied Engineering Science 2:341-327.

Schriener J, Doherty P (2015). Drones Show Potential to Aid Jobsite Safety and Efficiency”. Tech Trends”. Retrieved August 9, 2015, from http://enewsletters.constructionexec.com/techtrends/2013/07/drones-show-potential-to-aid-jobsite-safety-and-efficiency/

Snider M, Welch WM (2015). FAA shoots down Amazon’s drone delivery plans. Retrieved November 16, 2015, from http://www.usatoday.com/story/tech/2015/02/15/amazon-cool-to-drone-rules/23473791/

Wallace L, Lucieer A, Watson CS (2014). "Evaluating Tree Detection and Segmentation Routines on Very High Resolution UAV LiDAR data." IEE Transactions on Geoscience and Remote Sensing 52:12.

Related Journals: